NASA CONTRACTOR REPORT

NASA CR-2703

EXPERIMENTAL STUDY OF TRANSIENT DYNAMICS OF A FLEXIBLE ROTOR

D. H. Hibner and D. F. Buono

Prepared by
PRATT & WHITNEY AIRCRAFT
East Hartford, Conn. 06108
for Lewis Research Center

NATIONAL AERONAUTICS AND SPACE ADMINISTRATION • WASHINGTON, D. C. • JUNE 1976

1. Report No.	2. Government Accession No.	3. Recipient's Catalog No.
NASA CR-2703		

4. Title and Subtitle	5. Report Date
EXPERIMENTAL STUDY OF TRANSIENT DYNAMICS OF A FLEXIBLE ROTOR	June 1976
	6. Performing Organization Code

7. Author(s)	8. Performing Organization Report No.
D. H. Hibner and D. F. Buono	PWA-5333
	10. Work Unit No.

9. Performing Organization Name and Address	11. Contract or Grant No.
Pratt & Whitney Aircraft 400 Main Street East Hartford, Connecticut 06108	NAS3-18523
	13. Type of Report and Period Covered
12. Sponsoring Agency Name and Address	Contractor Report
National Aeronautics and Space Administration Washington, D.C. 20546	14. Sponsoring Agency Code

15. Supplementary Notes

Final Report. Project Manager, Albert F. Kascak, U.S. Army Air Mobility R&D Laboratory and Fluid System Components Division, Lewis Research Center, Cleveland, Ohio

16. Abstract

This report presents the results of an experimental program to investigate the transient response of a flexible rotor. The program consisted of a series of tests conducted on a rig with a rotor designed to operate above its first bending critical speed. The purpose of the tests was to obtain experimental data on the transient behavior of a flexible rotor under conditions simulating those which might occur in a jet aircraft engine. The scope of the program included tests to measure the response of both balanced and unbalanced rotors during steady-state operation, acceleration, deceleration, and simulated blade loss.

17. Key Words (Suggested by Author(s))	18. Distribution Statement
Transient response Blade loss Flexible rotor Rotor vibration	Unclassified - unlimited STAR category 37

19. Security Classif. (of this report)	20. Security Classif. (of this page)	21. No. of Pages	22. Price*
Unclassified	Unclassified	44	$4.00

* For sale by the National Technical Information Service, Springfield, Virginia 22161

TABLE OF CONTENTS

LIST OF ILLUSTRATIONS

LIST OF ILLUSTRATIONS (Cont'd)

LIST OF TABLES

SUMMARY

This report presents the results of experimental tests performed by Pratt & Whitney Aircraft in compliance with NASA Contract NAS3-18523. The purpose of the tests was to obtain experimental data on the transient behavior of a flexible rotor operated under conditions simulating those which might occur in a jet aircraft engine. The data will form the basis for correlation with theoretical results, and aid in the future development of aircraft rotors which are designed to operate above the first bending critical speed.

The program was conducted on a test rig with a single flexible rotor consisting of a 12.7 mm (.5 in) diameter shaft mounted on ball bearings 660 mm (26.0 in) apart. The shaft had five disks symmetrically placed with respect to the center of the bearing span. The shaft was driven by a variable speed hydraulic motor through a bellows coupling.

The contractual program included a series of experimental tests during which the response of the rotor was measured at or near each of the five disks.

The test program is summarized as follows:

STEADY STATE TEST

The steady-state response of the rotor system with .72 gm cm (.01 oz in) imbalance at the center disk was recorded at several speeds, both below and above the first bending critical speed of the system.

BLADE LOSS TEST

A 3.96 gm cm (.055 oz in) imbalance was suddenly applied to the center disk as the rotor was operated above its first bending critical speed. This simulated the loss of a blade from an engine rotor. The transient response of the rotor was recorded from approximately .18 seconds before blade loss to 1.87 seconds after.

ACCELERATION TEST

The rotor was accelerated at a known rate through the first bending critical speed and the transient response of the system was recorded. The test was repeated with the rig first in a balanced condition, and then with a .72 gm cm (.01 oz in) imbalance applied to the center disk.

DECELERATION TEST

The shaft was decelerated through the first bending critical speed at such a rate as to produce a measurable torsional windup of the shaft between the end disks, and the transient response of the system was measured. The test was repeated with the rig first in a balanced condition and then with 1.88 gm cm (.0261 oz in) imbalance applied to the center disk.

INTRODUCTION

This report presents the results of an experimental program to investigate the transient response of a flexible rotor. The work was conducted by Pratt & Whitney Aircraft under NASA Contract NAS3-18523. The program had two purposes. These are:

(1) To study experimentally the transient dynamics of a flexible rotor rig designed to simulate possible operating conditions of an aircraft engine, and

(2) To obtain experimental data on a flexible rotor for future comparison with theoretical prediction methods.

A flexible rotor, by definition, is one which operates above its first flexural natural frequency. Flexible rotors are of considerable interest in modern high speed gas turbine engine design, since they can contribute to reduced engine weight, improved aerodynamic performance, and lower overall engine cost. These benefits are a result of a simpler rotor and support structure design. Such a rotor mounted on only two bearings, instead of three or more, will produce considerable savings in weight and cost, and will improve performance because there will be fewer obstructions in the gaspath. In additon, reducing the number of bearings and bearing supports in a gas turbine engine increases dependability and ease of maintenance.

Flexible rotors, however, will have some inherent disadvantages. They will have more bending strain energy near the natural frequency (critical speed) than will a "stiff" rotor. As a result, such rotors will be more susceptible to high lateral and torsional deflection, clearance problems, and dynamic instability. They will also cause increased bearing loads; and, blade loss will be more critical. Sophisticated balancing techniques and means of providing damping on the bearing support structure will probably be needed to keep rotor amplitude to a minimum. However, since a flexible rotor offers many benefits in an engine, it is worthwhile to establish its limitations by rigorous experimental effort and associated development of analytical techniques.

The following text describes the behavior of a simply supported, two-bearing rotor. The testing conducted on this rotor system represents a basic step in building the required transient response technology because it provides experimental results for simply supported flexible rotors. Testing on this simple rotor affords an understanding of rotor dynamic transients which can be applied to more complex systems.

TECHNICAL PROGRAM

TEST SYSTEM

The test rig used in the program is shown in Figure 1. The rig has a single rotor with a 12.70 mm (.500 in) diameter solid steel shaft mounted on self-aligning ball bearings 660 mm (26.0 in) apart. A sketch of the system is shown in Figure 2. This shows the five disks which are symmetrically placed with respect to the center of the bearing span. Each of the center and end disks have 36 balance holes and the center disk is designed to release a balance weight to simulate blade loss. The end disks have high polar inertia in order to produce a gyroscopic stiffening effect. The high polar inertia also causes angular twist of the shaft when the shaft is subjected to rapid acceleration or deceleration torques. Each bearing is mounted in a sleeve which is fitted with a set of rubber "O" rings and supported by a rigid steel support pedestal. The "O" rings are used to provide support flexibility as well as damping for the otherwise lightly damped system. The shaft is driven by a variable speed hydraulic motor through a bellows coupling. The bellows coupling provides constant velocity and offers minimal shear and moment restraint to the shaft.

INSTRUMENTATION

Non-contacting proximity probes were used to measure vertical and horizontal shaft displacements at five locations along the shaft. The axial position of these probes is listed in Table I and shown schematically on Figure 2. For the steady state testing the displacement signals and a once-per-rev keyphasor signal were processed by a trim balance analyzer. This provides the running speed, the component of displacement synchronous with running speed, and the phase of the synchronous component. The information was displayed in digital form and was also available as a D.C. proportional voltage for plotting. All of the displacement signals for the transient testing were recorded by a high speed Data Memory System. Once stored in the memory system, the data was played back at a slower rate in analog form for plotting time traces and orbits.

The memory system consisted of a memory control module and thirteen memory modules. The system would process up to thirteen analog signals which were simultaneously sampled and converted to digital format over a preselected time interval. The signals were then stored as digital data over the duration of the time interval. Each analog signal was sampled and converted to digital data at a rate of 2000 samples per second. The individual memory modules (one per analog data channel) had a capacity of 4096 digital words which allowed a maximum sampling time interval of 2.048 seconds. Once the data was stored in the memory system it was output in analog form at a slower rate to facilitate plotting. A useful advantage of this system was that it allowed the data playback rate to be slowed down to 1/200 of the input rate without amplitude or time distortion.

The instantaneous velocity for the acceleration and deceleration tests was obtained by measuring the frequency of pulses created by proximity probes at the rims of the disks having 36 equally spaced balance holes. The angular twist of the rotor shaft during the rapid deceleration test was also obtained by recording the pulses generated by the equally spaced balance holes on the disks at the ends of the shaft. Proximity probes were located at each of the end disks and positioned such that the pulses created by each disk were in phase when the shaft was running at a constant speed. The angular twist was then obtained by measuring the rela-

tive shift between the pulse signals when the deceleration torque was applied. Since the acceleration and deceleration tests were of short duration, the high speed data memory system was also used to record the velocity and angular twist for these tests.

STEADY STATE ANALYSIS AND DYNAMIC MODEL

The test rig was modeled and analyzed on critical speed and forced response analysis programs. The initial design geometries and material properties were used to establish the first dynamic model from which the predicted system response was obtained. During fabrication and assembly of the test rig, static tests were conducted to establish the bearing support assembly stiffness. Upon completion of assembly, the system was balanced and run through its operating speed range with known imbalances applied at the center disk to establish the critical speeds and imbalance sensitivities. The analytical and experimental results thus obtained, together with analytical parametric studies conducted to establish the effect of variations of bearing support stiffness, shaft stiffness and support damping, were used to define the dynamic model of the system.

Figure 2 shows a schematic of the dynamic model. The lettered stations designate positions on the rotor shaft where external masses and inertias (disks, bearings and coupling) are attached. The sections between these stations were modeled as uniformly distributed masses and springs to simulate the uniform shaft between major masses. The bellows coupling was modeled by an equivalent spring mass system. The coupling mass is represented by the external mass at station "b". The coupling stiffness is represented by a rigid shaft section between stations "a" and "b" plus the equivalent springs K_3 (radial) and T_3 (torsional) at station "a". Table II lists the geometry and physical properties of the rig model.

Using this model, the first two forward and backward modes were predicted as a function of shaft speed. This is shown in Figure 3. The first forward synchronous mode is predicted at 2335 rpm and is a first bending mode as shown in Figure 4. The same system was analyzed by the linear forced response program. The synchronous response of the system to a .72 gm cm (.01 oz/in) imbalance at the center disk for speeds of 80, 95, 100 and 120 percent of the first forward critical is shown in Table III. The responses listed in this table are for shaft locations which are the same as those on the rig at which the vibration amplitudes were measured during testing.

BALANCING AND STEADY STATE TESTING

Preliminary analysis and testing showed the rig to be very sensitive to imbalance. Initial balancing was accomplished by using a two plane balancing procedure on the large end disks. Then, to achieve a better balanced condition, a single plane balance procedure was applied to the blade loss disk at the center of the shaft. The resulting balanced responses of the system for shaft speeds of 80, 95, 100 and 120 percent of the first critical are given in Table III. The state of balance was checked before each task in the program and fine adjustments were made.

After balancing, a .72 gm cm (.01 oz in) imbalance was added at the center disk mass and the rig was run at speeds of 80, 95, and 120 percent of the first critical speed. Vibration amplitudes were recorded at each of the proximity probe stations. For ease of comparison to the steady state analytical data and to account for residual imbalance and run-out, the

amplitude readings for the balanced tests were subtracted from the data for the unbalanced test. The resulting vibration amplitudes are given in Table III. A response plot was made of center disk synchronous vertical amplitude to document the peak response speed for the first critical during a slow acceleration of the shaft from 400 rpm to 2850 rpm. The response plot is shown in Figure 5. Two peak responses are shown on this figure. The first is the backward synchronous critical predicted at 1100 rpm which actually occurs at about 1080 rpm. The second is the first forward critical which occurs at approximately 2335 rpm as predicted.

BLADE LOSS TEST

The blade loss transient response test was run at 120 percent of the first bending critical speed. Two 3.26 gm cm (.055 oz in) balance weights were attached diametrically opposite each other on the rim of the center disk and the balanced response of the system was checked. The balanced system was then run to 2802 rpm and one of the rim balance weights was released to initiate the transient response simulating blade loss. The resulting transient response measured by all displacement probes was recorded by the high speed data memory system. The time duration of the measured response extended from approximately .18 seconds before blade loss to 1.87 seconds after blade loss. The second rim weight was then released to rebalance the system so that it could be safely decelerated.

The time traces of the displacement signals for each of the displacement probes are shown on Figures 6, 7, 8, 9 and 10. Figure 11 shows orbit traces of the center disk for the steady state before blade loss as well as sixteen cycles after blade loss. Both the time traces and orbit traces indicate that the system response exhibits a beating phenomenon. This can be explained by the fact that the shaft is whirling simultaneously at both the turning frequency and the first bending natural frequency several hundred rpm lower. The general expression for the system response after blade loss can be written as

$$R = A \sin(\omega t + \phi) + Be^{-\lambda t} \sin(\omega_c t + \phi_c)$$

The first term is the steady state response of amplitude, A, and phase, ϕ, due to the resulting imbalance rotating at the turning frequency, ω. The second term is the decaying transient response of amplitude, $Be^{-\lambda t}$, and phase, ϕ_c. The frequency of the transient component is the first bending natural frequency, ω_c. The response can be rewritten as

$$R = \bar{R} \sin(\omega t + \phi - \alpha),$$

where

$$\bar{R} = [A^2 + (Be^{-\lambda t})^2 + 2ABe^{-\lambda t} \cos(\Delta\omega t + \Delta\phi)]^{1/2},$$

$$\Delta\omega = \omega - \omega_c \quad ,$$

$$\Delta\phi = \phi - \phi_c \quad ,$$

$$\alpha = \text{Arc Tan} \left[\frac{Be^{-\lambda t} \sin(\Delta\omega t + \Delta\phi)}{A + Be^{-\lambda t} \cos(\Delta\omega t + \Delta\phi)} \right]$$

This expression shows that the response is an amplitude modulated Sine function; and, the beat phenomenon is due to the fact that the modulation function, $\bar{R}$, is cyclic. $\bar{R}$ is not precisely periodic because of the exponential decay term, $e^{-\lambda t}$, which does not repeat with

time. When the decay rate is small, the amplitude modulation appears periodic and beating is evident. By neglecting the effect of the decay term, the beat frequency is $\Delta\omega$, which is the difference between the turning frequency and the natural frequency. In addition, the analytical expression for the system response shows that the phase angle, α, will vary with time at the same frequency as $\Delta\omega$.

The time traces in Figure 8 show that the period of the amplitude modulation is approximately 0.23 seconds. This results in a beat frequency of 261 cycles/minute. The critical speed map in Figure 3 indicates that at the blade loss test speed of 2802 rpm, the first bending natural frequency is 2525 rpm. The difference frequency is, therefore, 277 cycles/minute which agrees well with the observed beat frequency.

Figure 12 shows photos of the scope display of the time traces of all of the displacement probe signals. These time traces have once-per-rev keyphasor marks on them which show that the phase of the vibration does not remain constant, but rather varies in the time similar to the decay envelope of the amplitude signal.

ACCELERATION TEST

The acceleration test was run with the system in both balanced and unbalanced conditions. During the balancing procedure for this part of the program, it was observed that the peak response speed of the system shifted approximately 1.3% from 2335 rpm to 2365 rpm. The cause for this apparent change in critical speed is not specifically known. It is possibly caused by minimal changes in the damping and stiffness characteristics of the rig.

In both the balanced and unbalanced tests, the shaft was accelerated from below 80% to above 120% of the first bending critical to attain a constant acceleration between the limits of 80% and 120% of the critical. The horizontal and vertical displacement signals at four of the displacement probe stations and the angular velocity of the end disks were recorded by the high speed data memory system. The displacement signals from displacement probes 1 and 2 were not recorded.

The time trace of the shaft angular velocity during the balanced accelerations test is shown on Figure 13. The trace shows that the acceleration from 80% to 120% of the first critical took approximately 1.1 seconds. It also shows by virtue of its linearity that the angular acceleration was constant at 90 rad/sec^2 (859 rpm/sec). The angular acceleration of the shaft was calculated from the velocity signals by differentiating the velocity curves with respect to time. The velocity and acceleration measured at the two gyro disks and the blade loss disk were identical to velocity data presented. The time traces of the displacements are shown on Figure 14. These traces show a small response throughout the speed range. It should be noted, however, that the maximum response over the speed range is slightly larger than the steady state balanced response and generally occurs at a higher speed; i.e. the response lags the speed. Figure 15 shows photos of the displacement time traces with keyphasor marks superimposed. These traces show a phase shift as the amplitude goes beyond the peak value and starts to decrease. The phase traces also show that the phase shift is much more pronounced for the horizontal than the vertical.

The unbalanced acceleration test was run with a .72 gm cm (.01 oz in) imbalance added to the center disk. The time trace of the shaft angular velocity for this test shown on Figure 13 shows that the acceleration from 80% to 120% of the first bending critical took approximately 1.1 seconds. This velocity trace also shows constant angular acceleration of 90 rad/sec^2 (859 rpm/sec). The velocity and acceleration measured at the two gyro disks and the blade loss disk were identical to the velocity data presented. The time traces of the displacement probe signals are shown in Figures 16 and 17. A comparison of the center disk displacement time traces in Figure 16 to the shaft velocity time trace in Figure 13 shows that the center disk amplitude peaks out at 2560 rpm (108% of the critical speed), thus the response again lags the speed. The peak-to-peak amplitude of the center disk at this time is about .305 mm (.012 in) which is less than half of the maximum steady state amplitude at the critical speed (Figure 5 and Table III). Figure 18 shows photos of the displacement time traces with keyphasor marks superimposed. Unlike those of the balanced acceleration test, these phase traces indicate a phase shift occurring for both the horizontal and vertical displacement signals.

The acceleration test was run a total of three times to check for repeatability. All tests showed system response in excellent agreement with the reported data.

DECELERATION TEST

In the deceleration test portion of the program, the shaft was decelerated from 120% to 80% of the first critical at such a rate as to produce a measurable torsional windup of the shaft between the end disks. The test was run with the rig in both balanced and unbalanced conditions. The vertical and horizontal displacements were recorded at all displacement probe locations. The velocity and acceleration were monitored at the two end disks and at the center disk.

Obtaining a balanced state of the rig for the deceleration tests was more difficult than for the other portions of the test program. This has been presumed due to an unwanted effect of the drive coupling which produced large amplitudes during deceleration tests. An acceptable level of balance was finally achieved in which the amplitude growth during deceleration did not exceed 150% of the steady state response at 120% of the first critical. The unbalanced deceleration test was run with 1.88 gm cm (.0261 oz in) imbalance added to the center disk. In this part of the program as in the acceleration test, the steady state peak response speed was at 2365 rpm.

The time traces of the velocity during the balanced and unbalanced deceleration tests are shown on Figures 19 and 20. The measured velocity did not vary over the length of the shaft. Therefore, the velocity traces shown represent the velocity at all stations. The angular acceleration over the speed range was calculated by differentiating the velocity traces with respect to time. The calculated acceleration for the balanced and unbalanced tests are also shown on Figures 19 and 20.

The angular twist of the shaft during the rapid deceleration was obtained by measuring the phase shift between the pulse signals generated by the proximity probes aimed at the balance holes in the end disks. Due to the high pulse frequency (1419 pulses per second at 2365 rpm) and the resulting high pulse density, it was not possible to obtain angular twist

measurements continuously over the entire deceleration range. As a result, the twist measurements were made by looking at pulses generated in .0205 second time intervals at five different speeds in the deceleration speed range. The resulting calculated twist angles are plotted on Figure 21. The twist angles were calculated for the balanced deceleration test. A comparison of the velocity and acceleration traces in Figures 19 and 20 indicates that the angular twist will be the same for the unbalanced as for the balanced test. Comparing the angular twist to the angular acceleration rates for the two deceleration tests shows that the maximum twist occurs at the same time as the maximum acceleration and, in general, the twist is proportional to the acceleration rate.

The displacement time traces for the balanced and unbalanced deceleration tests are shown in Figures 22, 23, 24, 25 and 26. Comparison of the center disk displacement trace for the balanced deceleration test with its corresponding velocity trace shows that the maximum center disk amplitude occurs at a speed of 2680 rpm (.6% above the critical speed). Making the same type of comparison for the unbalanced deceleration test shows that the maximum center disk amplitude occurs at a speed of 2250 rpm (4.9% below the critical speed). Further comparison of the balanced and unbalanced acceleration rates and twist angles to the respective maximum displacements shows that the maximum displacements occur significantly later than the maximum shaft twist or angular acceleration.

The maximum center disk amplitude for the unbalanced test is about .63 mm (.025 in) which is less than half of steady state peak response with the same amount of unbalance applied. The photos on Figures 27 and 28 show the center disk displacement traces for both the balanced and unbalanced tests with once-per-revolution keyphasor marks superimposed. These photos show cyclic phase shift throughout the deceleration. The deceleration test was run three times to check system repeatability; and, as in the case of the acceleration test, all tests were in excellent agreement with the reported data.

CONCLUDING REMARKS

Before a viable flexible rotor can be designed into an engine, a complete definition of the rotor's behavior under both normal and abnormal engine operating conditions is required. This definition is fundamental to the development and advancement of flexible rotor technology. An understanding of flexible rotor behavior, and the ability to predict that behavior under any loading condition, will permit design modifications to reduce rotor amplitude and decrease the dynamic loading on the support structures, thereby increasing its fatigue life. The loading conditions which are of most importance to nearly all rotor systems include suddenly applied imbalance, suddenly applied torques, loads imposed by maneuvers, internally generated loads such as compressor surge and, of course, normal rotor imbalance. The effects of non-linear bearing and damping devices must be included in the prediction system since these items are common and necessary. With the development of critical speed analyses, steady state and transient response analyses, and rotor/bearing stability analyses, the flexible rotor behavior can be defined. The experimental results and information presented in this report will assist significantly in understanding the dynamics of flexible rotors.

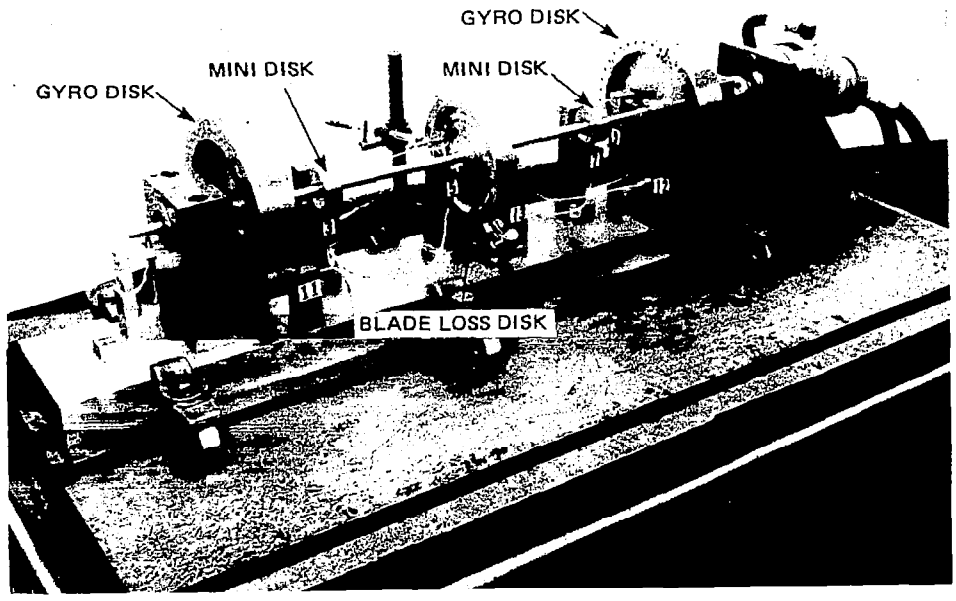

FIG. 1 TEST RIG DESIGNED FOR TRANSIENT TESTING AT SPEEDS ABOVE THE FIRST BENDING CRITICAL SPEED

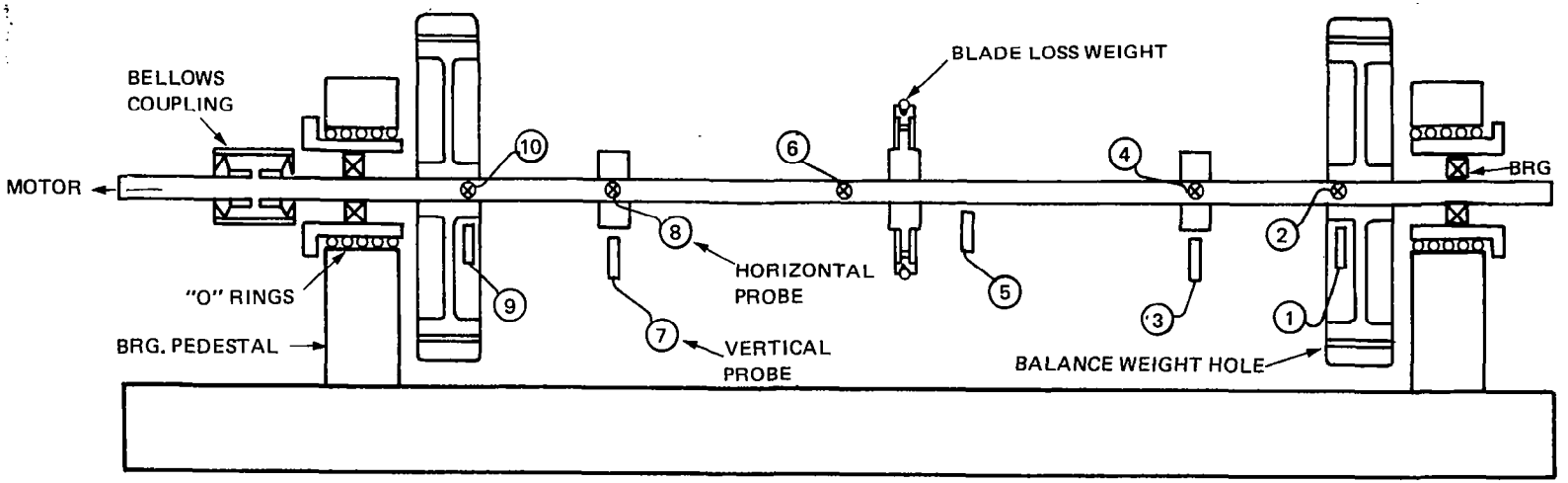

TEST RIG SKETCH

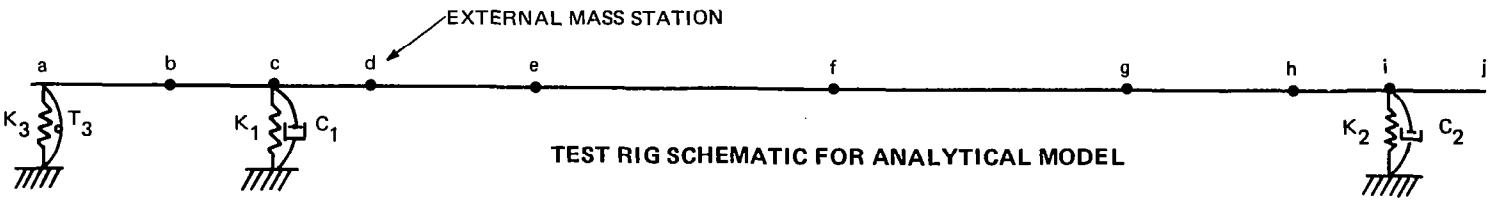

TEST RIG SCHEMATIC FOR ANALYTICAL MODEL

FIG. 2 SKETCH OF TEST RIG AND SCHEMATIC OF ANALYTICAL MODEL

DATA STATION		1		2		3		4		5	
PROBE NUMBER		1	2	3	4	5	6	7	8	9	10
DIRECTION		VERT	HORIZ	VERT	HORIZ	VERT	HORIZ	VERT	HORIZ	VERT	HORIZ
AXIAL	IN.	23.364	23.364	20.264	20.264	14.200	11.900	6.136	6.136	2.636	2.636
LOCATION	CM.	59.345	59.345	51.471	51.471	36.068	28.194	15.858	15.858	6.695	6.695

TABLE I DISPLACEMENT PROXIMITY PROBE LOCATION AND ORIENTATION

	ROTOR STATION	AXIAL LOCATION		EXTERNAL WEIGHT		POLAR MASS MOMENT OF INERTIA I_P		TRANSVERSE MASS MOMENT OF INERTIA I_T	
		IN	CM	LB	Kg	LB-IN^2	Kg - CM^2	LB-IN^2	Kg-CM^2
	a	-5.110	-12.979	0.0	0.0	0.0	0.0	0.0	0.0
COUPLING	b	-1.500	-3.810	.112	.0544	.020	.0585	.010	.0293
NO. 1 BEARING	c	0.0	0.0	.271	.1229	.1094	.3201	.0547	.1601
GYRO DISK	d	2.136	5.425	11.440	5.1891	122.80	359.36	63.198	184.94
MINI DISK	e	6.160	15.646	.4984	.2261	.2174	.6362	.1321	.3866
BLADE LOSS DISK	f	13.000	33.020	.4636	.2103	.3257	.9531	.4280	1.2525
MINI DISK	g	20.140	51.156	.4984	.2261	.2174	.6362	.1321	.3866
GYRO DISK	h	23.864	60.615	11.440	5.1891	122.80	359.36	63.198	184.94
NO. 2 BEARING	i	26.000	66.740	.271	.1129	.1094	.3201	.0547	.1601
SHAFT END	j	27.500	69.850	0.0	0.0	0.0	0.0	0.0	0.0

SHAFT CHARACTERISTICS
DIA = 12.70 MM (.500 IN) DENSITY = 7.83 X 10^{-3} KG/CM^3 (.283 LB/IN^3)
MODULUS = 19.65 X 10^6 N/CM^2 (28.5 X 10^6 LB/IN^2)

SUPPORT CHARACTERISTICS

K_1 = 25796 N/CM (14730 LB/IN) C_1 = 14.0 $\frac{\text{N-SEC}}{\text{CM}}$ (8.0 $\frac{\text{LB-SEC}}{\text{IN}}$)

K_2 = 28003 N/CM (15990 LB/IN) C_2 = 14.0 $\frac{\text{N-SEC}}{\text{CM}}$ (8.0 $\frac{\text{LB-SEC}}{\text{IN}}$)

K_3 = 30.6 N/CM (17.5 LB/IN)

T_3 = 89.8 N-CM/RAD (7.95 LB-IN/RAD)

TABLE II TEST RIG PHYSICAL PROPERTIES FOR ANALYTICAL MODEL SHOWN IN FIG. 2

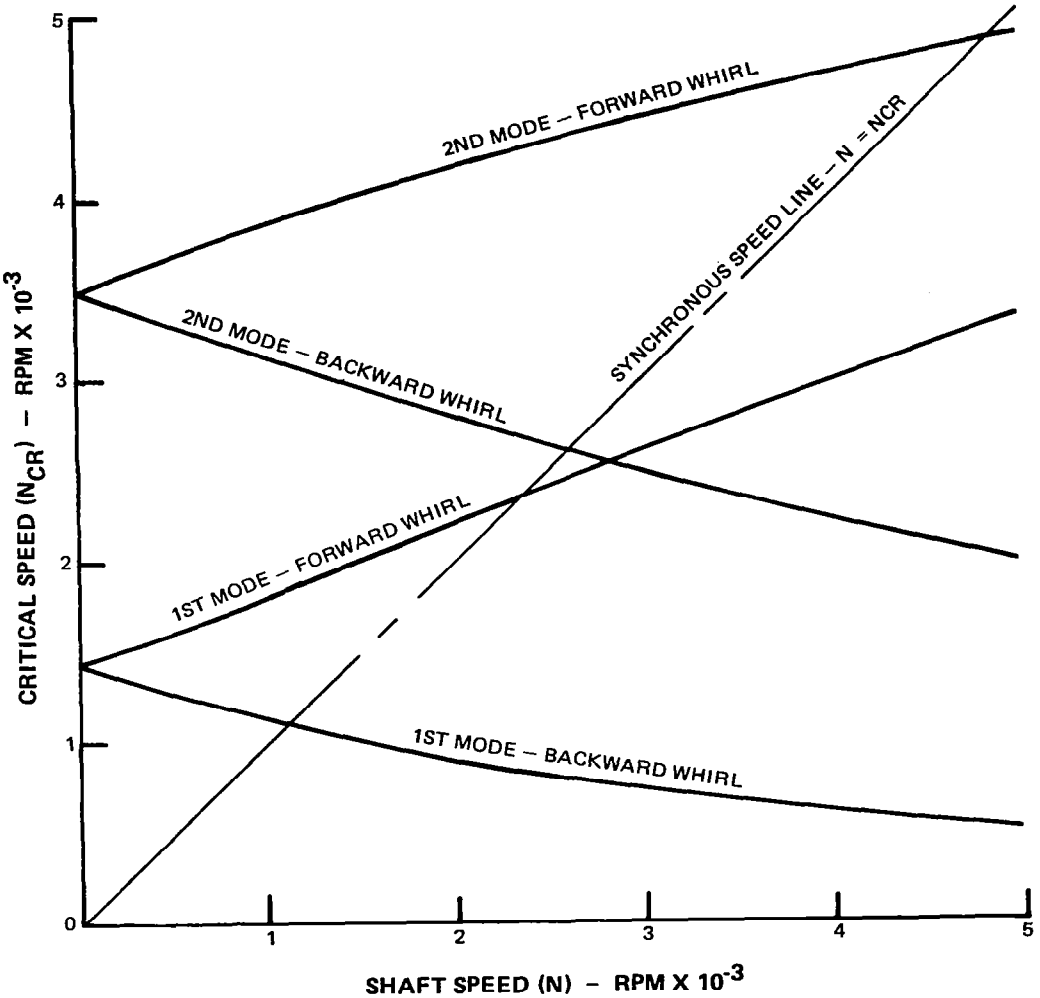

FIG. 3 ANALYTICALLY PREDICTED CRITICAL SPEED MAP

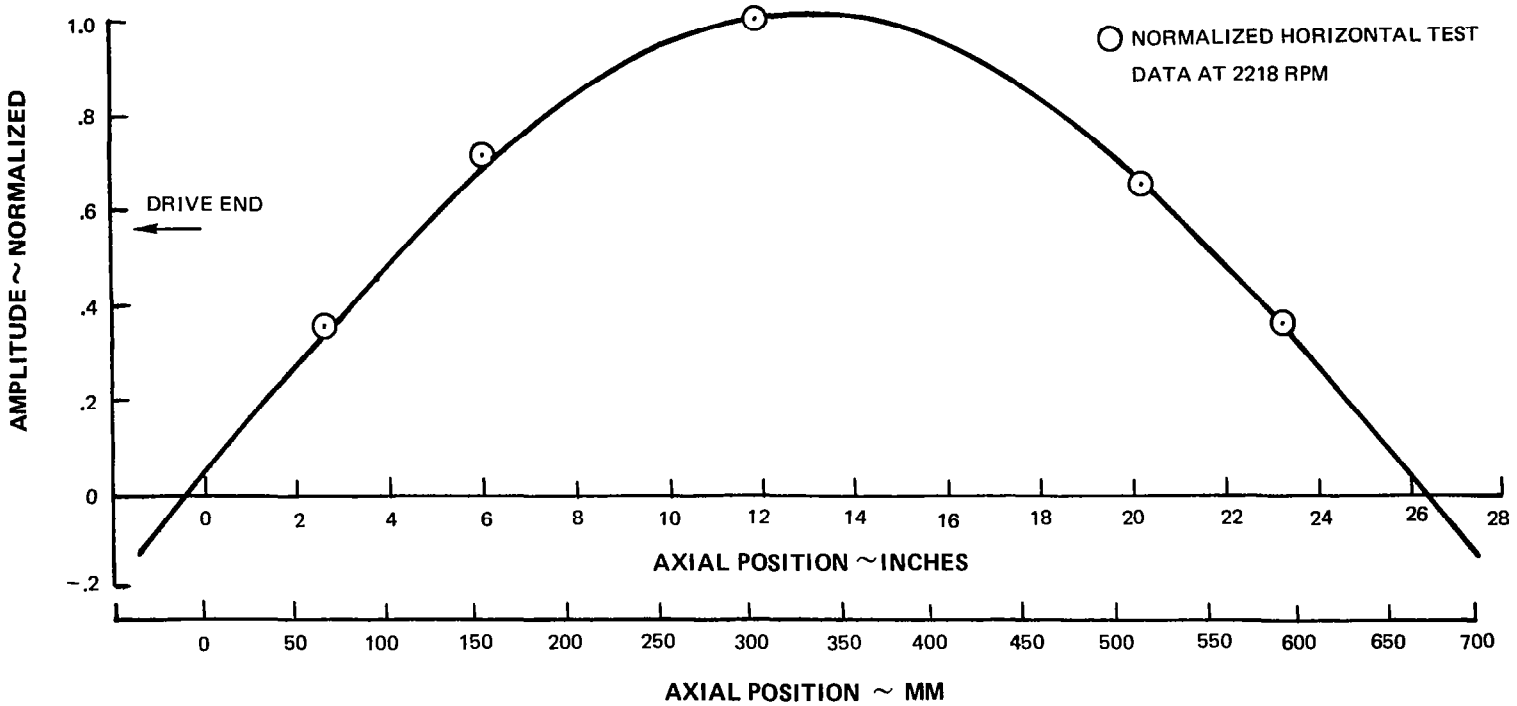

FIG. 4 PREDICTED FIRST BENDING MODE SHAPE

			DATA STATION	1		2		3		4		5	
			PROBE NUMBER	1	2	3	4	5	6	7	8	9	10
			DIRECTION	VERT	HORIZ	VERT	HORIZ	VERT	HORIZ	VERT	HORIZ	VERT	HORIZ
RESPONSE AT 1868 RPM (.8 N_{CR})	EXPERIMENTAL BALANCED	AMPL	IN X 10^3	.84	.65	.40	.40	.65	.51	.65	.43	.37	.23
			MM X 10^2	2.13	1.65	1.02	1.02	1.65	1.30	1.65	1.09	.94	.74
		PHASE	DEGREES	222	115	73	6	13	327	318	231	303	133
	EXPERIMENTAL IMBALANCED	AMPL	IN X 10^3	.39	.37	.74	.97	1.24	1.11	.78	.85	.36	.41
			MM X 10^2	.99	.94	1.88	2.46	3.15	2.82	1.98	2.16	.91	1.04
		PHASE	DEGREES	84	351	94	7	93	0	90	357	91	359
	PREDICTED IMBALANCED	AMPL	IN X 10^3	.390	.390	.730	.730	1.110	1.110	.755	.755	.303	.303
			MM X 10^2	.99	.99	1.85	1.85	2.82	2.82	1.92	1.92	.77	.77
		PHASE	DEGREES	88	358	88	358	89	359	88	358	88	358
RESPONSE AT 2218 RPM (.95 N_{CR})	EXPERIMENTAL BALANCED	AMPL	IN X 10^3	.91	.76	.67	.98	.58	.62	.47	.28	.34	.28
			MM X 10^2	2.31	1.93	1.70	2.49	1.47	1.57	1.19	.71	.86	.71
		PHASE	DEGREES	204	103	112	28	62	5	306	193	283	165
	EXPERIMENTAL IMBALANCED	AMPL	IN X 10^3	1.69	1.91	3.38	3.43	5.21	5.33	3.48	3.81	1.79	1.88
			MM X 10^2	4.29	4.85	8.59	8.71	13.23	13.54	8.84	9.68	4.55	4.78
		PHASE	DEGREES	102	9	103	10	99	9	101	9	99	11
	PREDICTED IMBALANCED	AMPL	IN X 10^3	1.940	1.940	3.530	3.530	5.320	5.320	3.670	3.670	1.509	1.509
			MM X 10^2	4.93	4.93	8.97	8.97	13.51	13.51	9.32	9.32	3.83	3.83
		PHASE	DEGREES	79	349	79	349	80	350	79	349	79	349
RESPONSE AT 2335 RPM (N_{CR})	EXPERIMENTAL BALANCED	AMPL	IN X 10^3	1.14	.93	.50	.81	.19	.49	.93	.81	.63	.71
			MM X 10^2	2.90	2.36	1.27	2.06	.48	1.24	2.36	2.06	1.60	1.80
		PHASE	DEGREES	211	112	161	59	226	98	279	163	267	159
	PREDICTED IMBALANCED	AMPL	IN X 10^3	9.430	9.430	17.025	17.025	25.480	25.490	17.700	17.700	7.360	7.360
			MM X 10^2	23.95	23.95	43.24	43.24	64.72	64.74	44.96	44.96	18.69	18.69
		PHASE	DEGREES	9	279	9	279	10	280	9	279	8	278
RESPONSE AT 2802 RPM (1.2 N_{CR})	EXPERIMENTAL BALANCED	AMPL	IN X 10^3	.708	.68	.66	.98	1.04	.78	1.19	1.11	.70	.78
			MM X 10^2	1.80	1.73	1.68	2.49	2.64	1.98	3.02	2.82	1.78	1.98
		PHASE	DEGREES	206	97	80	3	15	282	315	222	300	203
	EXPERIMENTAL IMBALANCED	AMPL	IN X 10^3	.73	.76	1.44	1.52	2.03	2.00	1.41	1.50	.70	.79
			MM X 10^2	1.85	1.93	3.66	3.86	5.16	5.08	3.58	3.81	1.78	2.01
		PHASE	DEGREES	265	178	269	171	259	170	261	169	259	173
	PREDICTED IMBALANCED	AMPL	IN X 10^3	.720	.720	1.250	1.250	1.820	1.820	1.305	1.305	.571	.571
			MM X 10^2	1.83	1.83	3.18	3.18	4.62	4.62	3.31	3.31	1.45	1.45
		PHASE	DEGREES	276	186	276	186	277	187	276	186	275	185

*ALL AMPLITUDES ARE PEAK TO PEAK

(EXPERIMENTAL IMBALANCE RESPONSE IS CHANGE IN RESPONSE DUE TO 0.72 g. cm. IMBALANCE AT CENTER DISK)

TABLE III TEST RIG STEADY STATE AMPLITUDES – ANALYTICALLY PREDICTED AND EXPERIMENTALLY OBSERVED

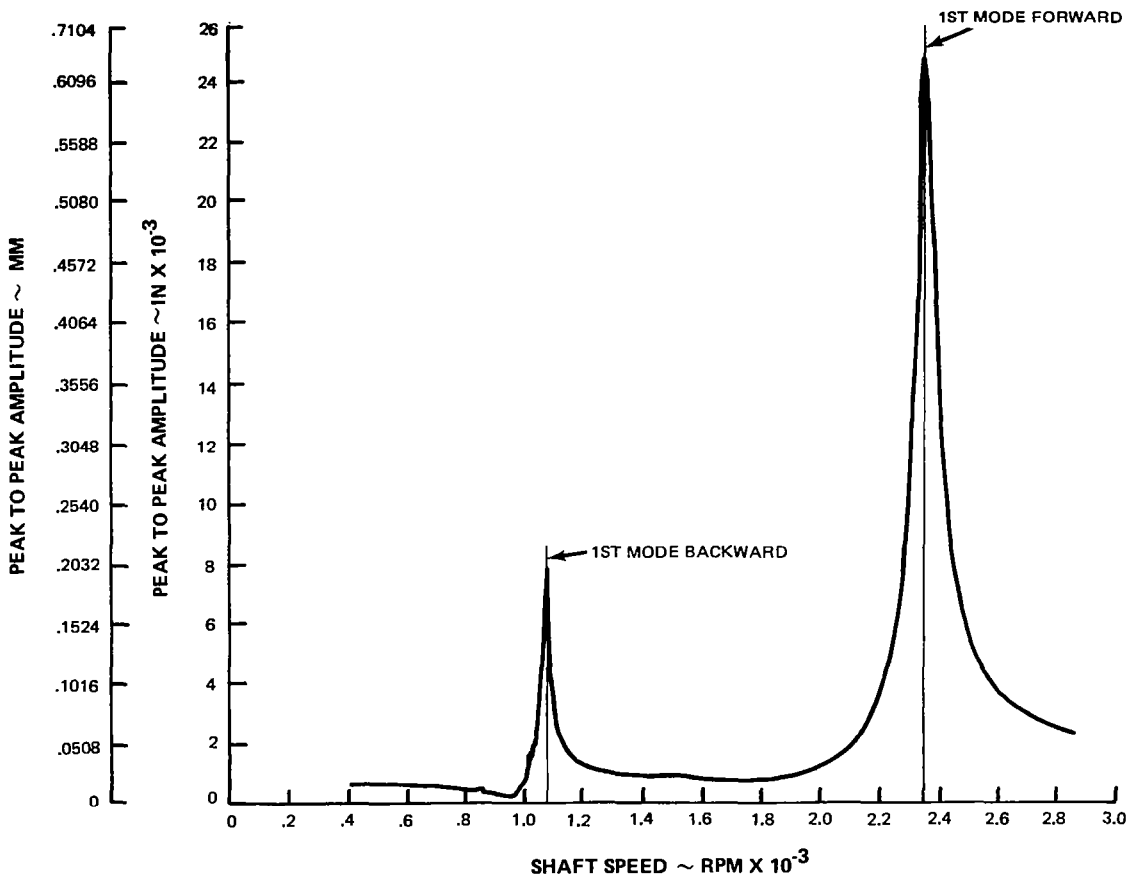

FIG. 5 VERTICAL STEADY STATE RESPONSE AT DATA STATION 3 .72 gm cm (.01 oz in) IMBALANCE APPLIED ON BLADE LOSS DISK

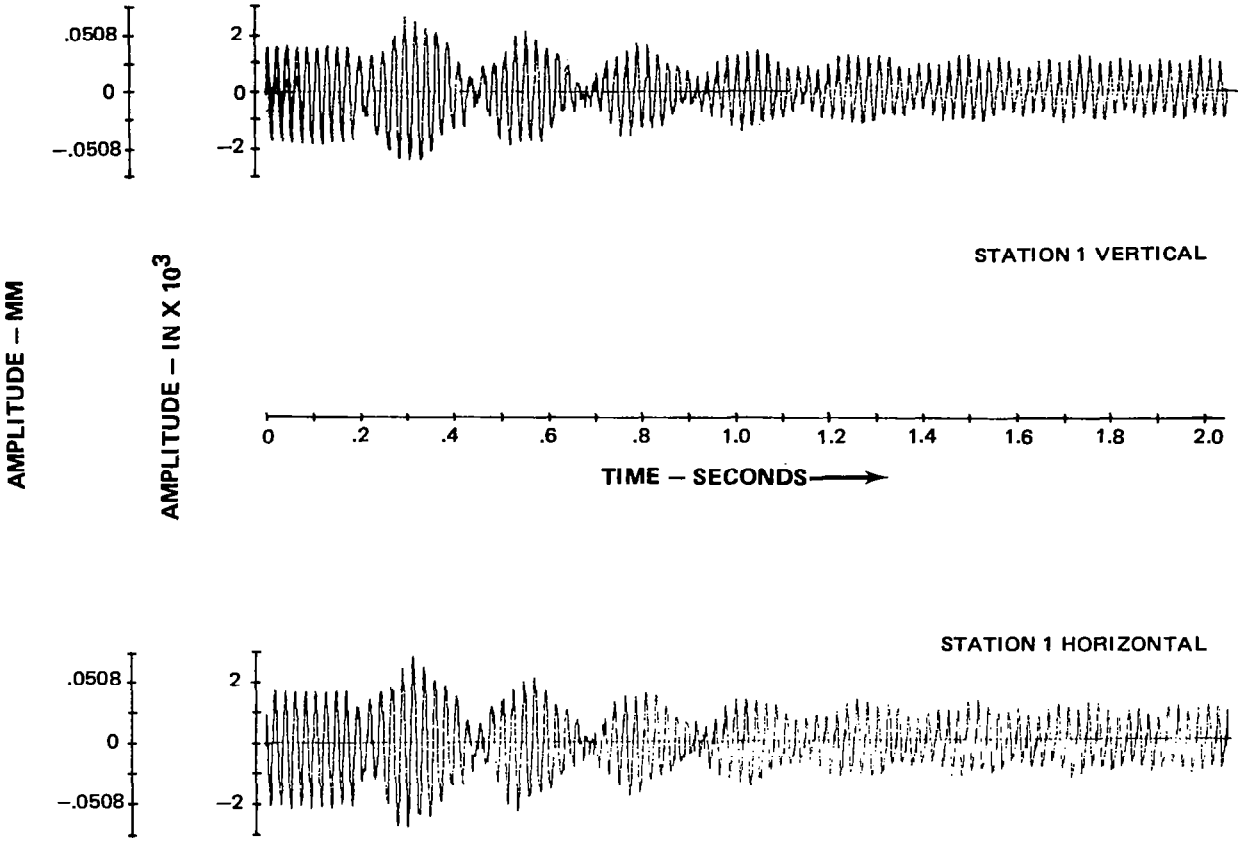

FIG. 6 DISPLACEMENT TIME TRACES FROM DATA STATION 1 DURING BLADE LOSS TEST

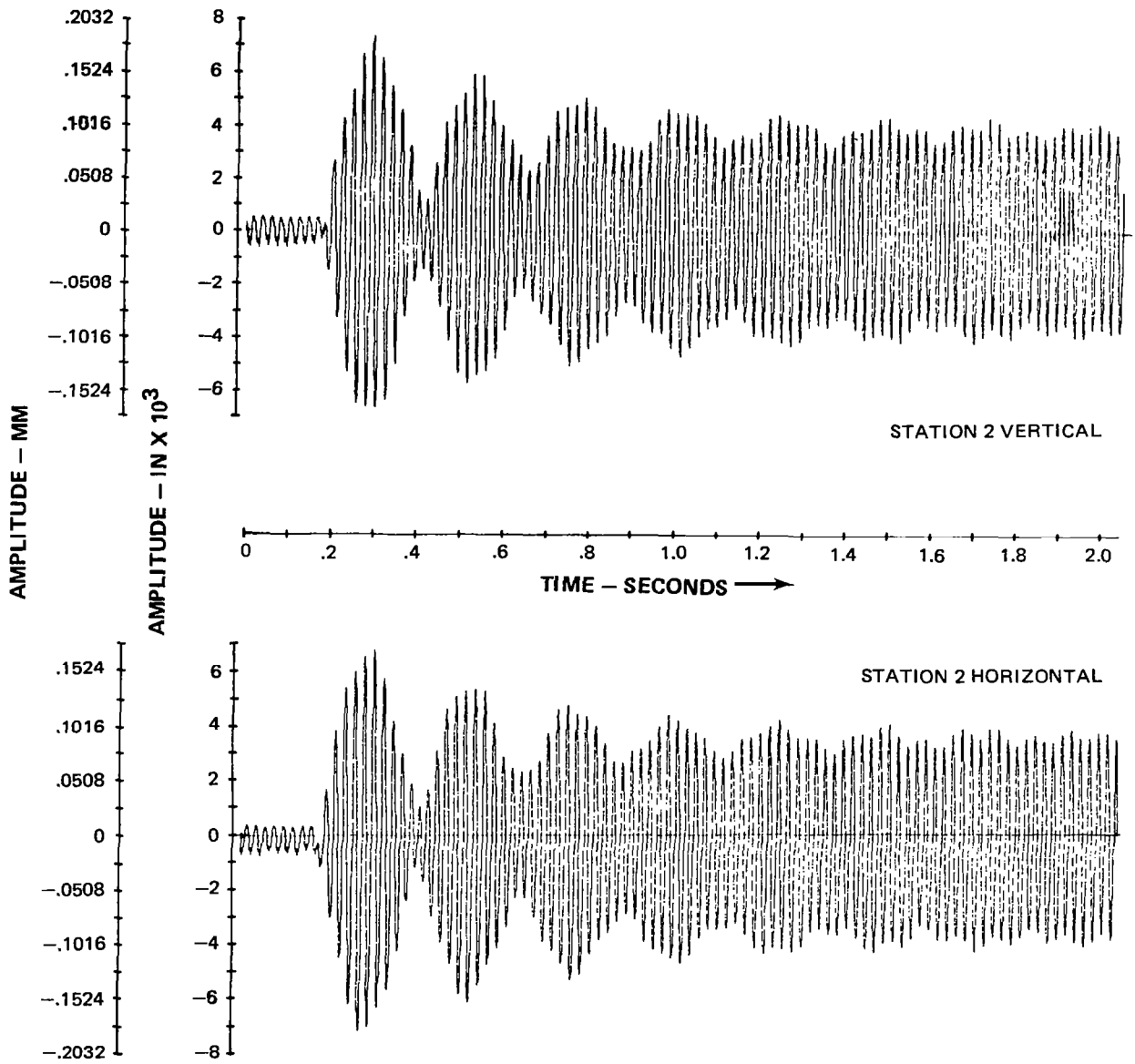

FIG. 7 DISPLACEMENT TIME TRACES FROM DATA STATION 2 DURING BLADE LOSS TEST

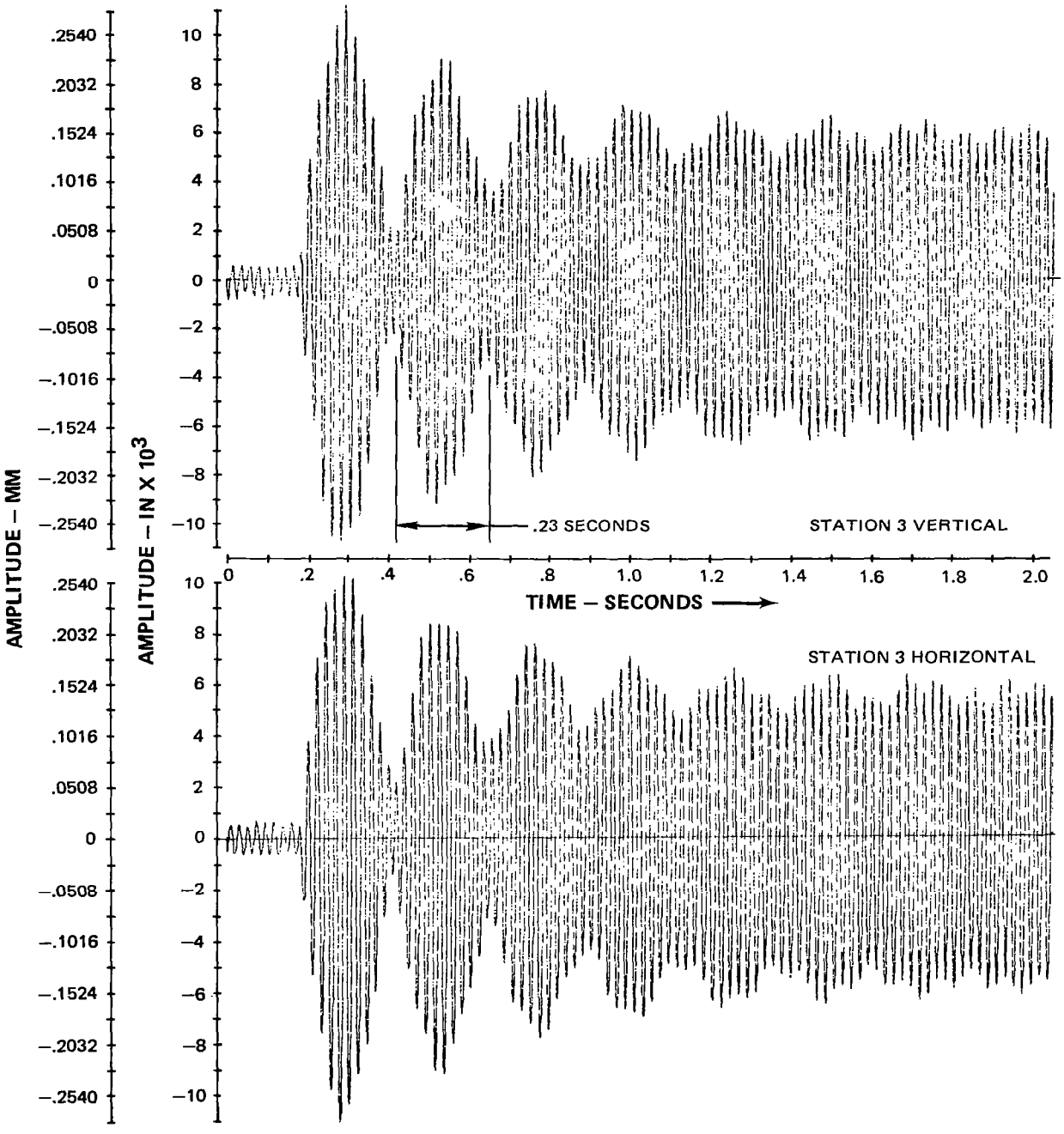

FIG. 8 **DISPLACEMENT TIME TRACES FROM DATA STATION 3 DURING BLADE LOSS TEST**

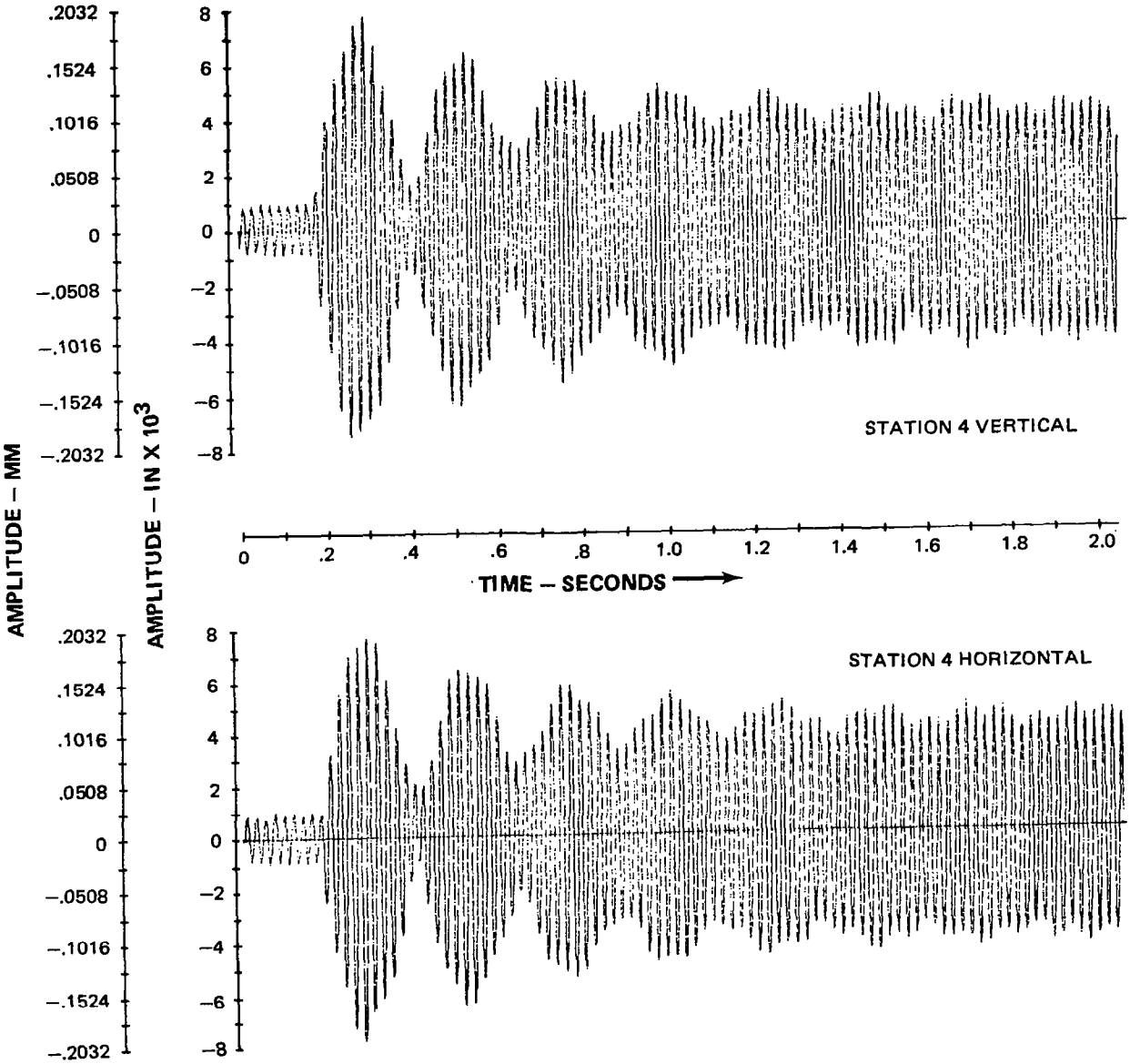

FIG. 9 DISPLACEMENT TIME TRACES FROM DATA STATION 4 DURING BLADE LOSS TEST

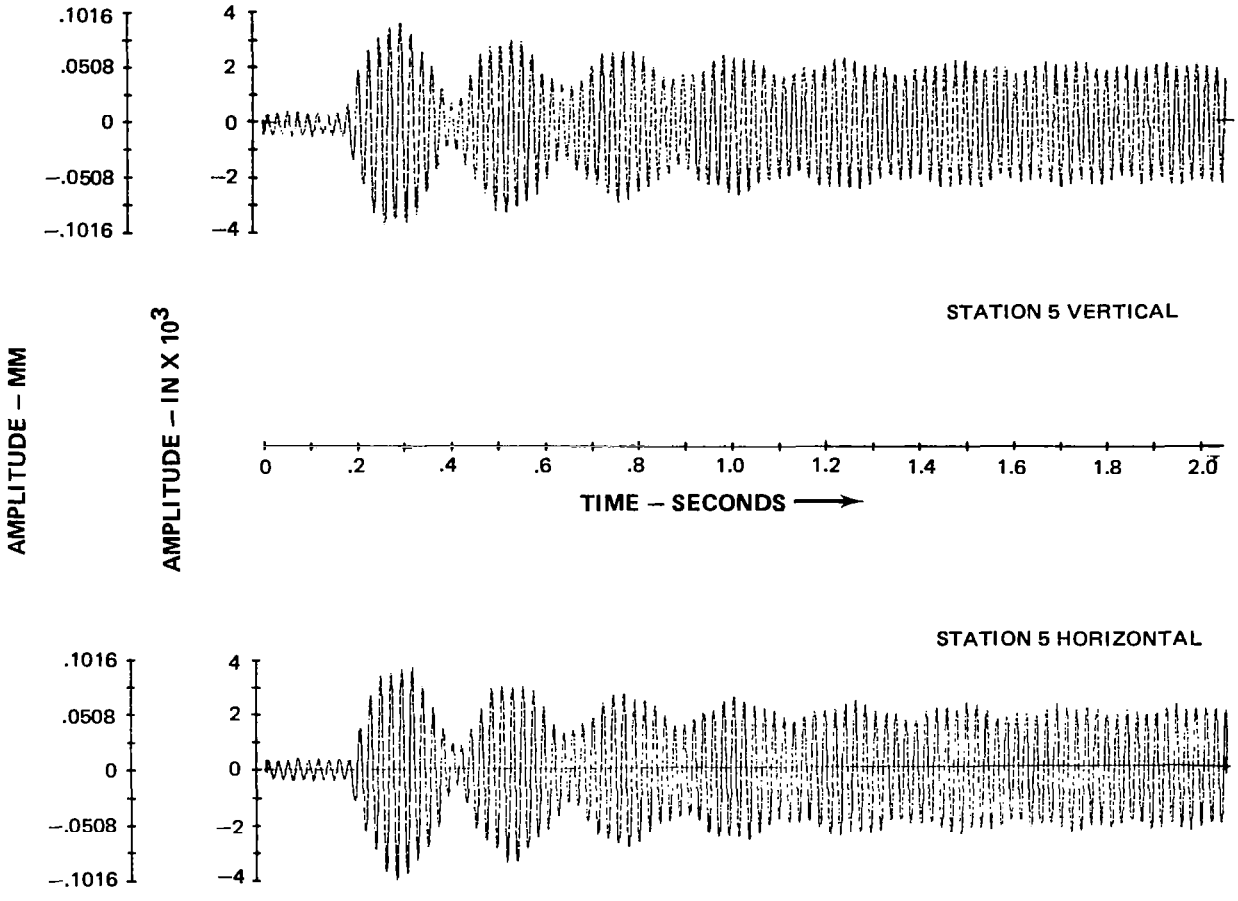

FIG. 10 **DISPLACEMENT TIME TRACES FROM DATA STATION 5 DURING BLADE LOSS TEST**

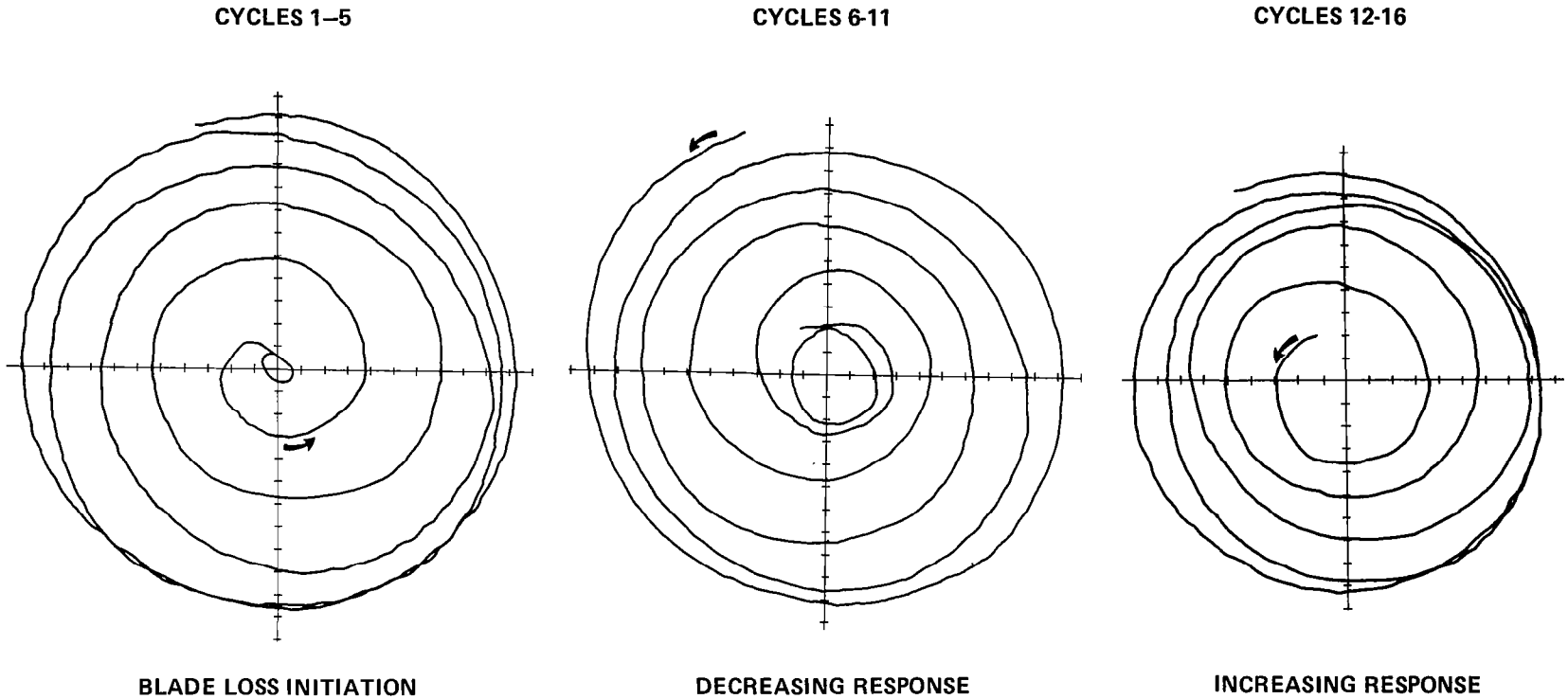

FIG. 11 ORBIT TRACES FROM DATA STATION 3 DURING FIRST SIXTEEN CYCLES AFTER BLADE LOSS INITIATION, AMPLITUDE SCALE .0254 MM(.001IN.) PER DIVISION

STATION 1 VERTICAL

STATION 5 VERTICAL

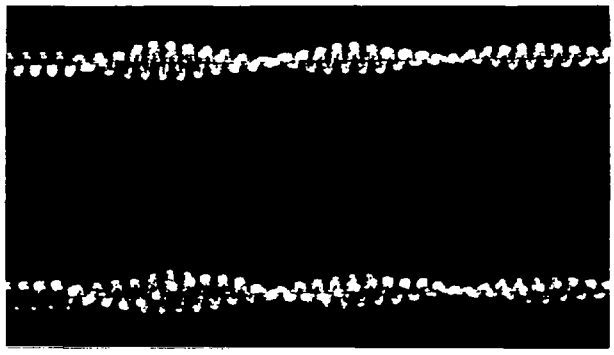

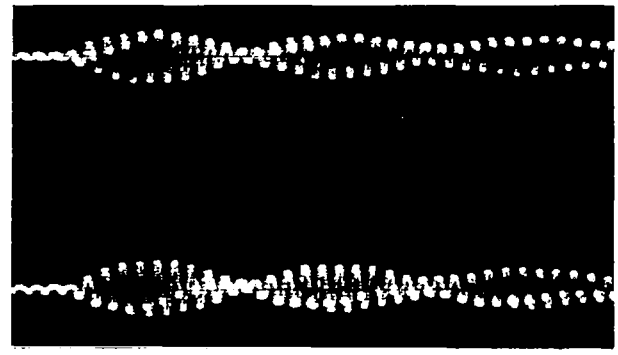

STATION 1 HORIZONTAL

STATION 5 HORIZONTAL

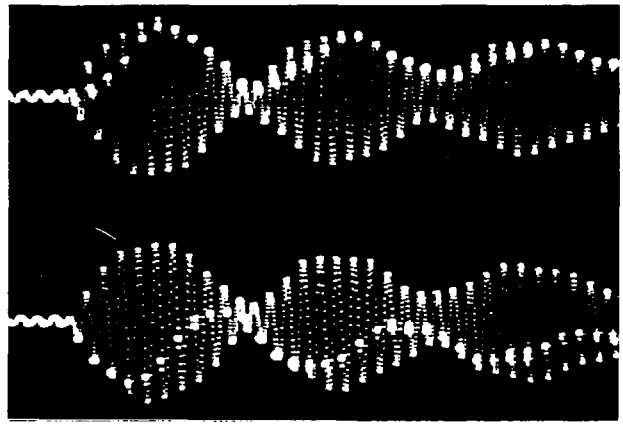

STATION 3 VERTICAL

STATION 3 HORIZONTAL

STATION 2 VERTICAL

STATION 4 VERTICAL

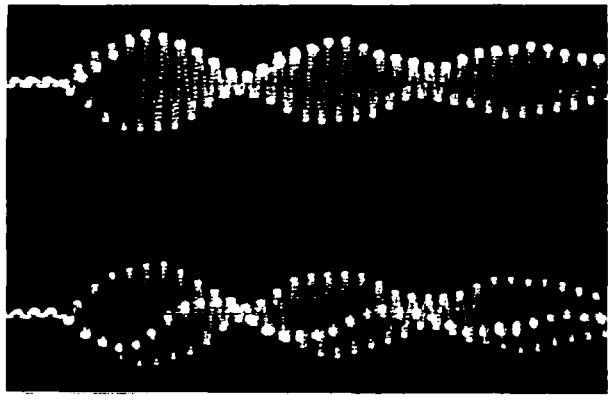

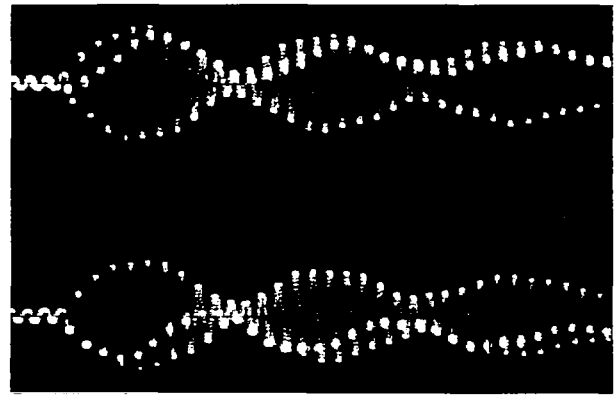

STATION 2 HORIZONTAL

STATION 4 HORIZONTAL

FIG. 12 DISPLACEMENT TIME TRACES WITH KEYPHASOR MARKS DATA STATIONS 1, 2, 3, 4 AND 5 DURING BLADE LOSS TEST

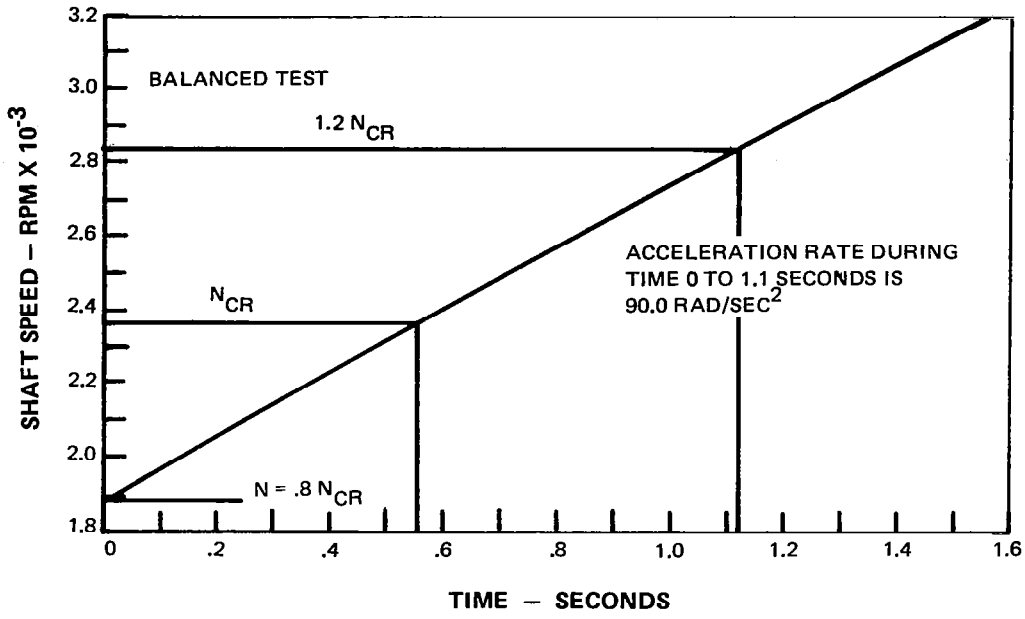

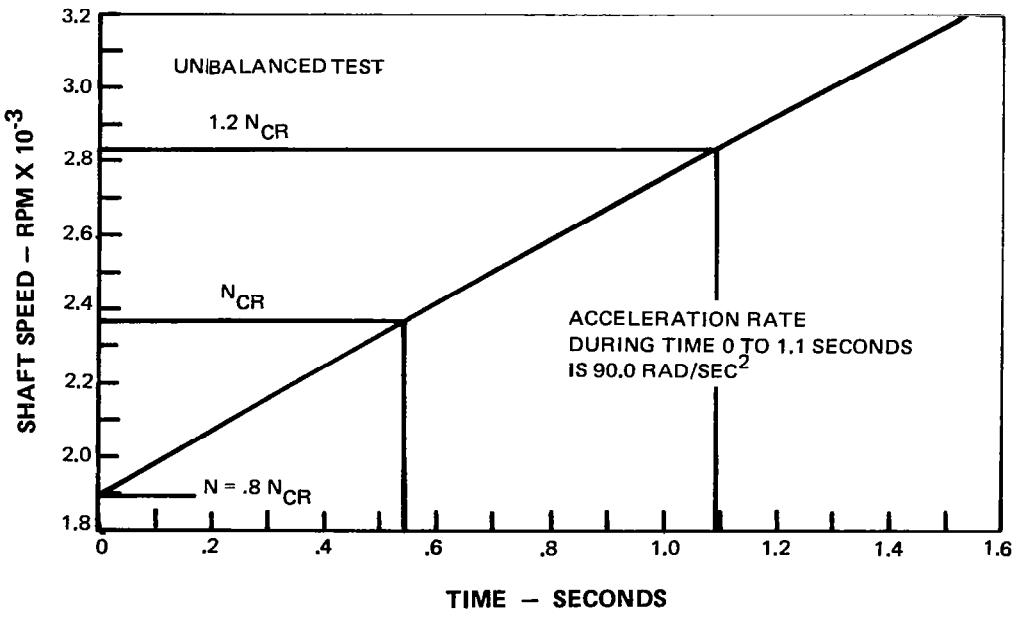

FIG. 13 SHAFT SPEED DURING BALANCED AND UNBALANCED ACCELERATION TEST

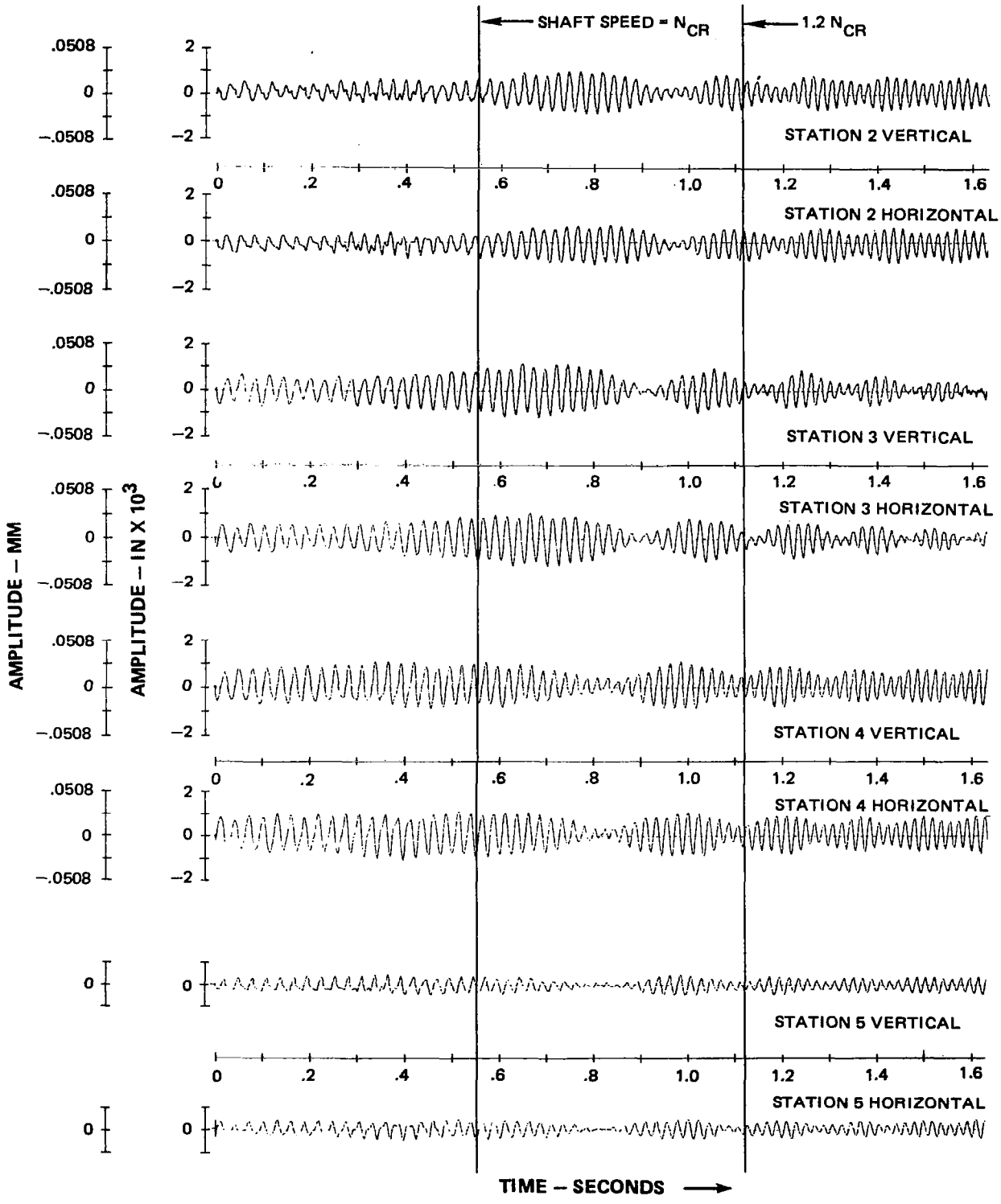

FIG. 14 DISPLACEMENT TIME TRACES FROM DATA STATIONS 2, 3, 4 AND 5 DURING BALANCED ACCELERATION TEST

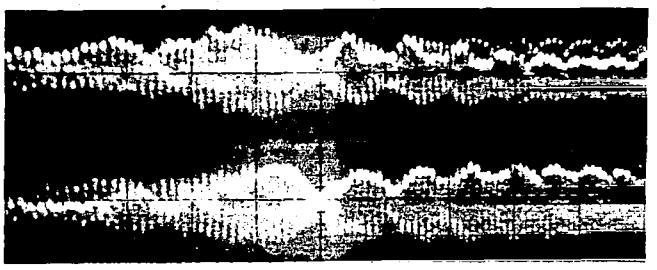

VERTICAL

HORIZONTAL

STATION 2

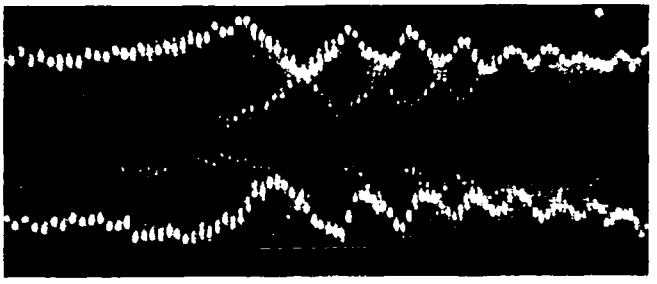

VERTICAL

HORIZONTAL

STATION 3

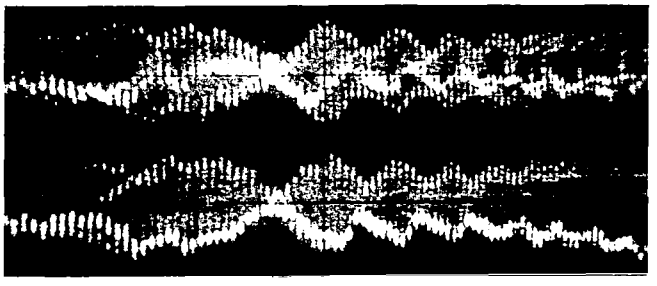

VERTICAL

HORIZONTAL

STATION 4

VERTICAL

HORIZONTAL

STATION 5

FIG. 15 DISPLACEMENT TIME TRACES WITH KEYPHASOR MARKS, DATA STATIONS 2, 3, 4 AND 5 DURING BALANCED ACCELERATION TEST

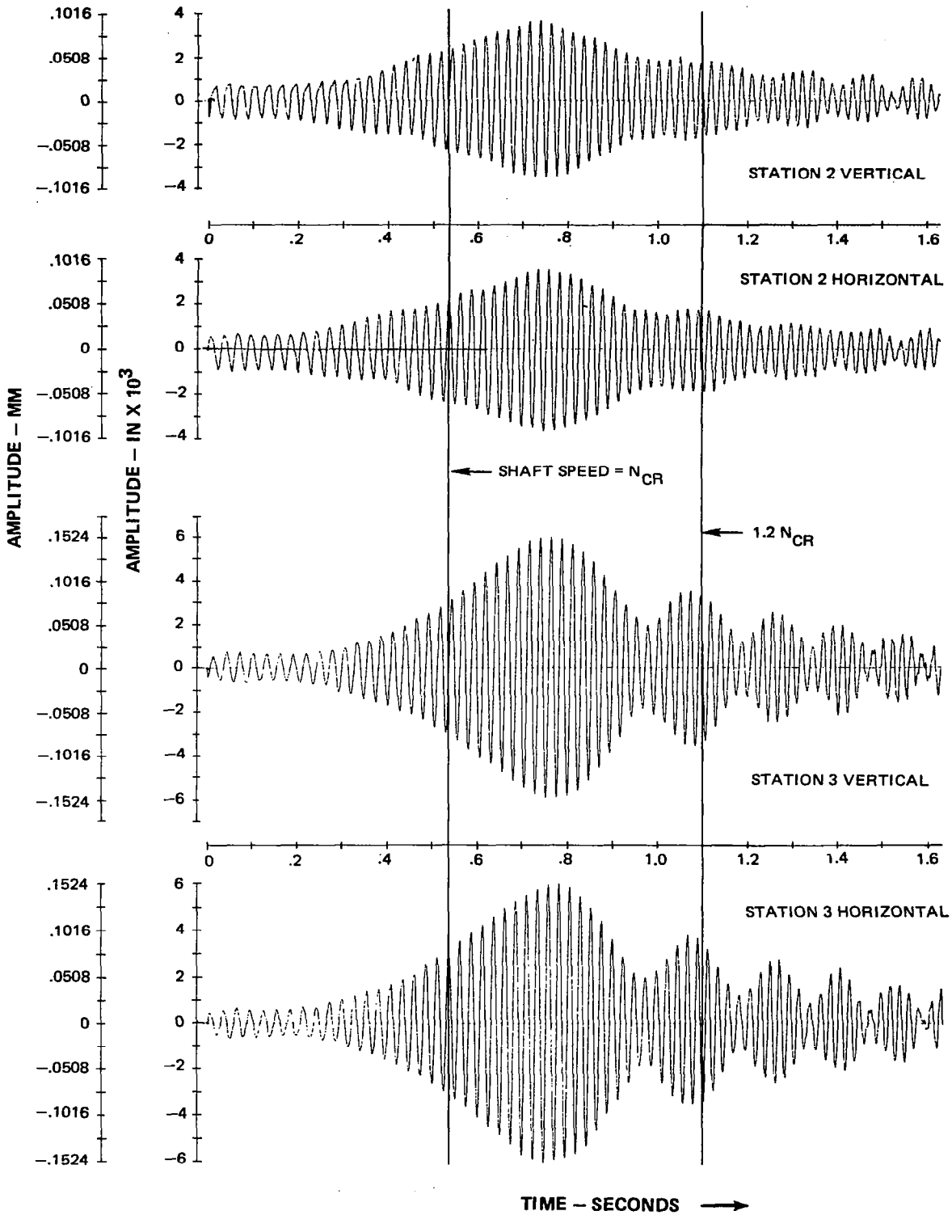

FIG. 16 DISPLACEMENT TIME TRACES FROM DATA STATIONS 2 AND 3 DURING UNBALANCED ACCELERATION TEST

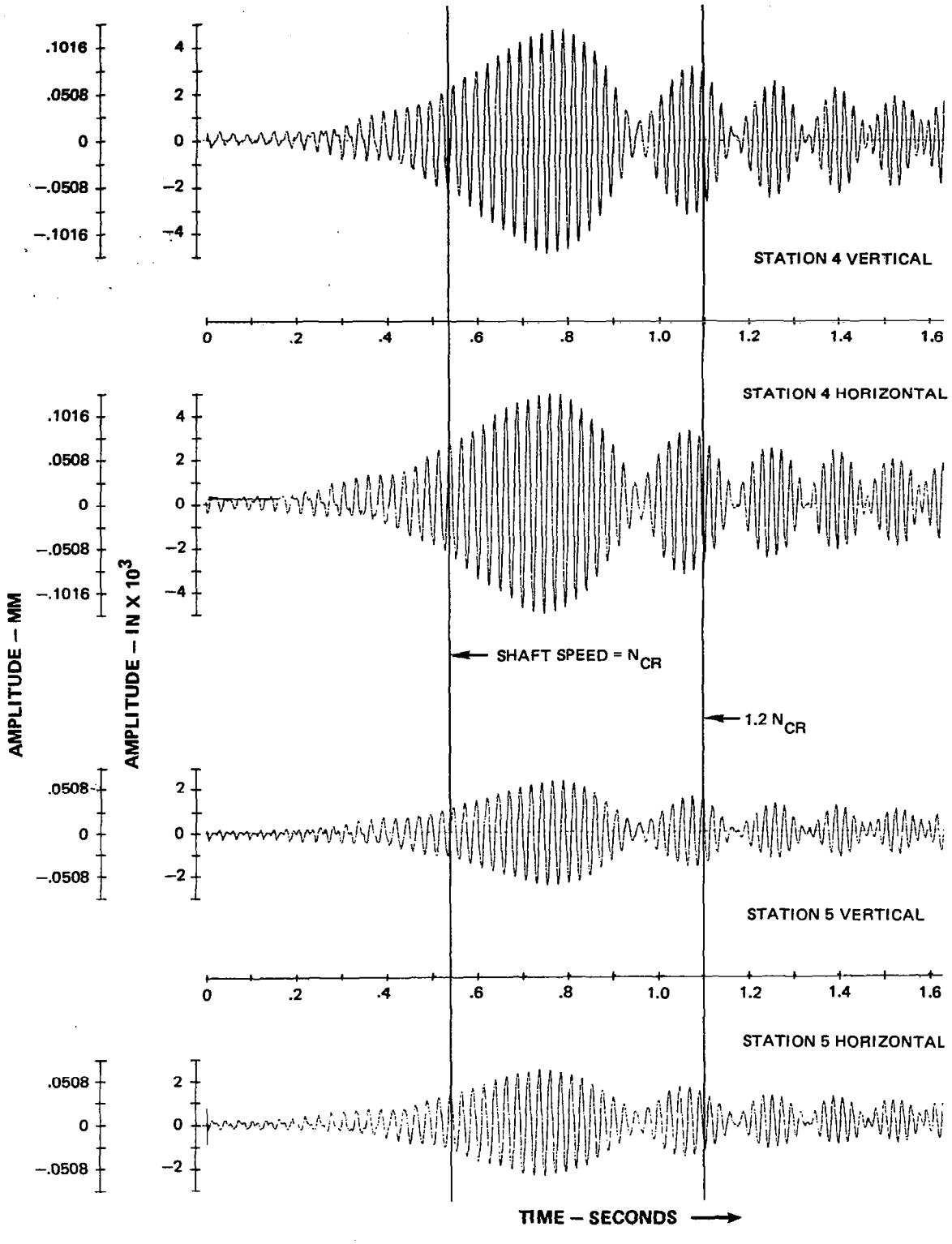

FIG. 17 DISPLACEMENT TIME TRACES FROM DATA STATIONS 4 AND 5 DURING UNBALANCED ACCELERATION TEST

STATION 2 VERTICAL

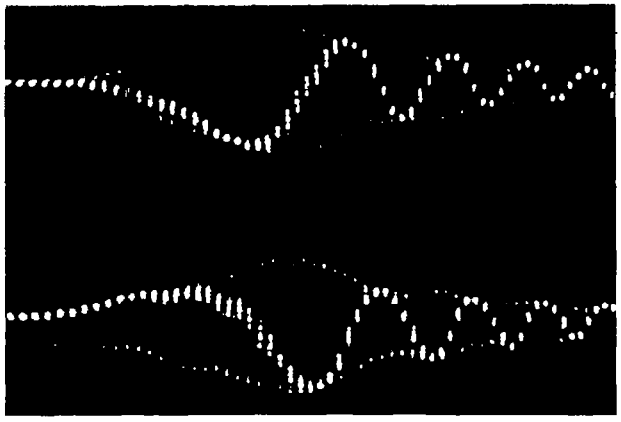

STATION 2 HORIZONTAL

STATION 3 VERTICAL

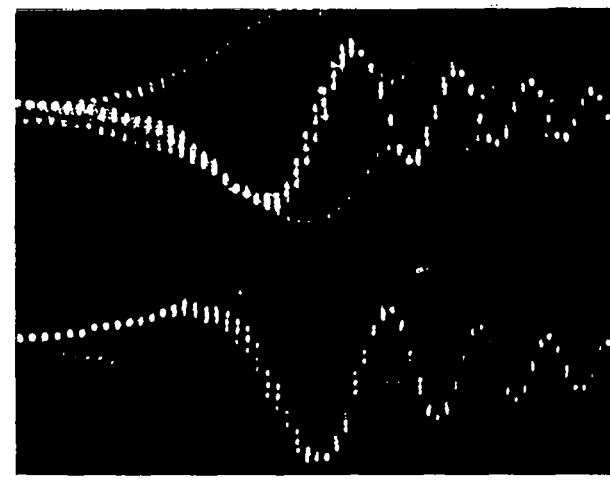

STATION 3 HORIZONTAL

STATION 4 VERTICAL

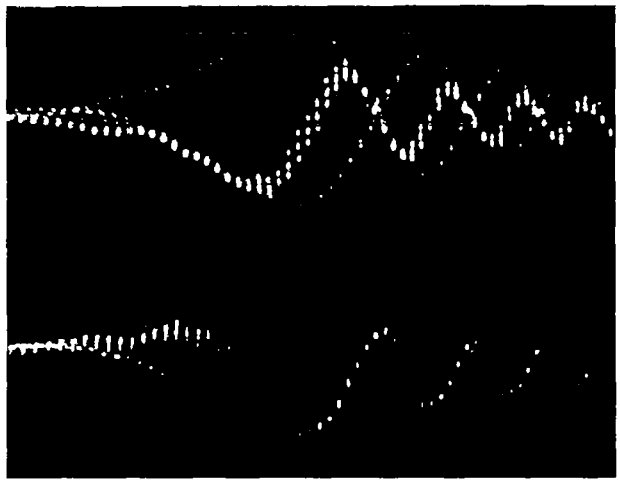

STATION 4 HORIZONTAL

STATION 5 VERTICAL

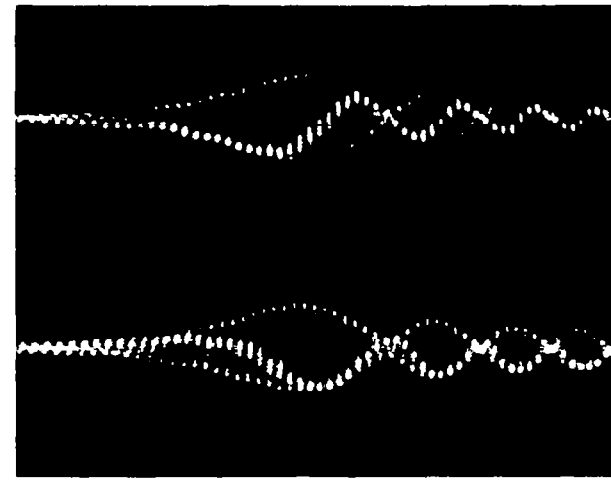

STATION 5 HORIZONTAL

FIG. 18 DISPLACEMENT TIME TRACES WITH KEYPHASOR MARKS, DATA STATIONS 2, 3, 4 AND 5 DURING UNBALANCED ACCELERATION TEST

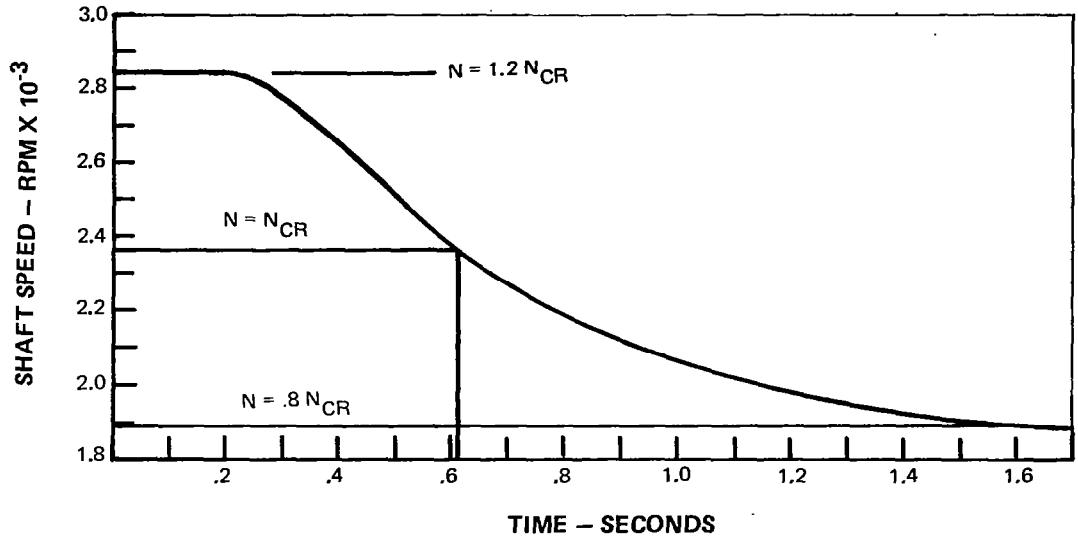

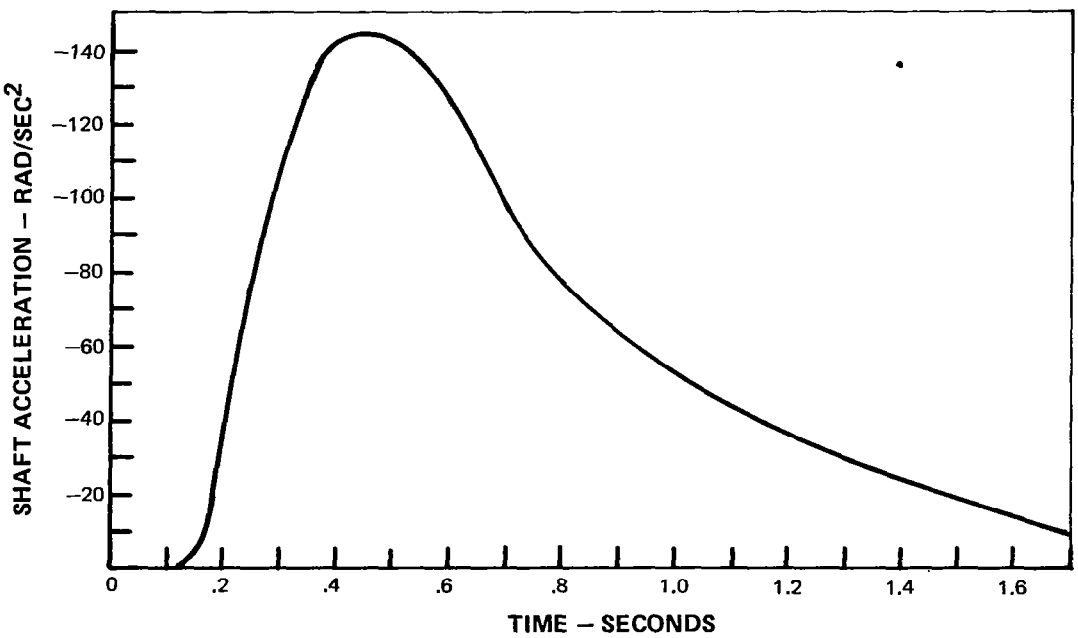

FIG. 19 SHAFT SPEED AND ACCELERATION DURING BALANCED DECELERATION TEST

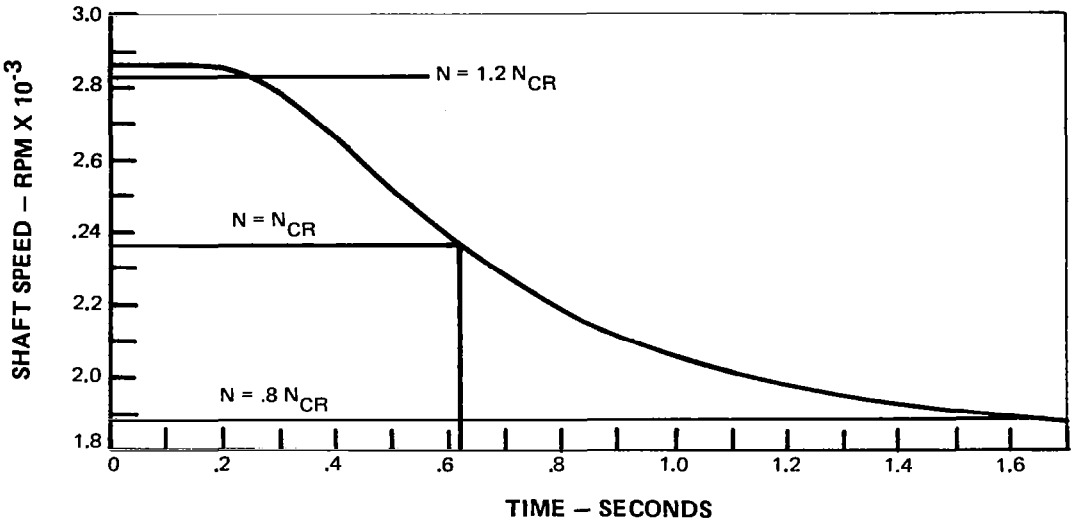

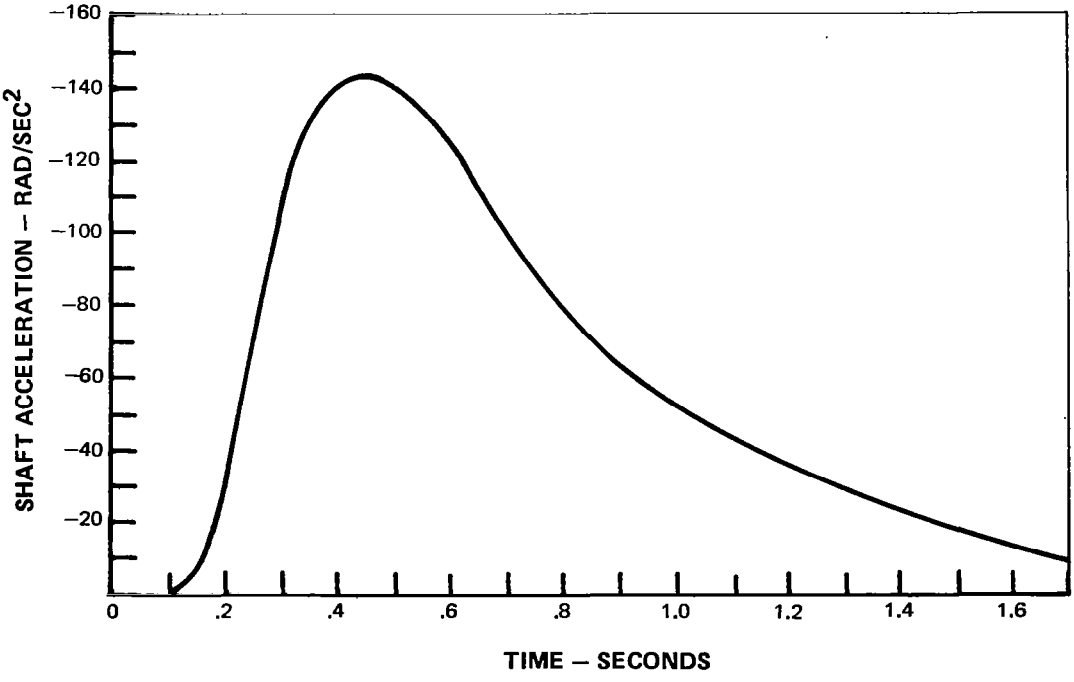

FIG. 20 SHAFT SPEED AND ACCELERATION DURING UNBALANCED DECELERATION TEST

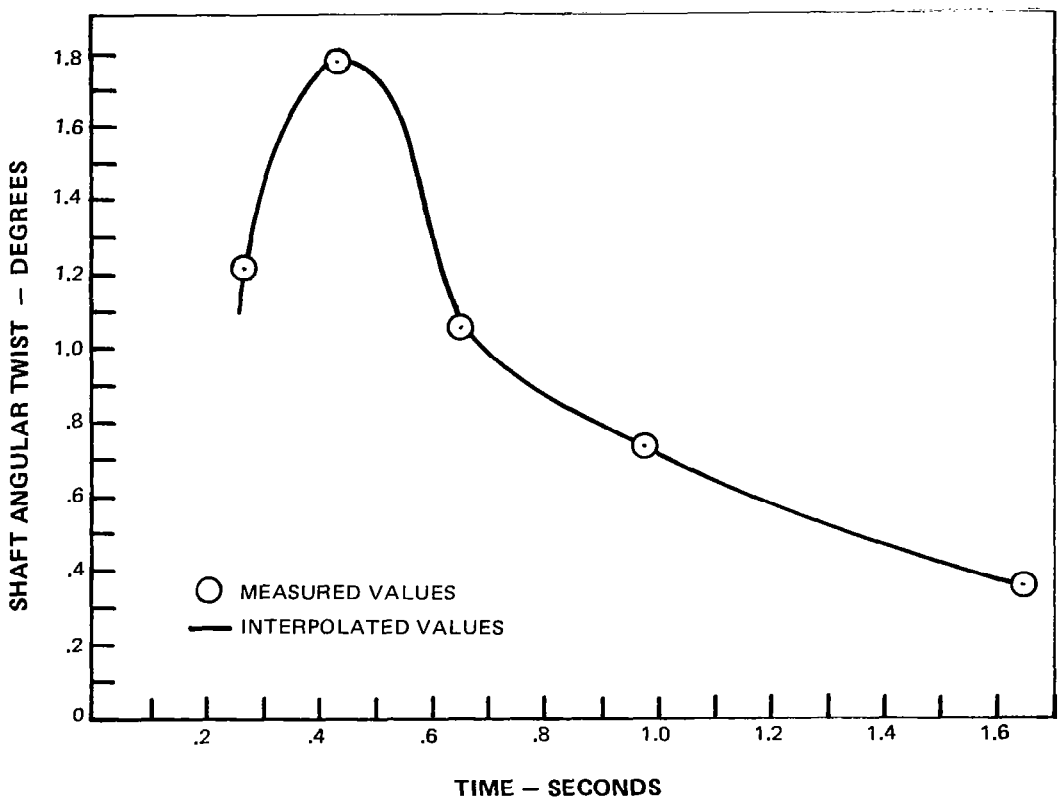

FIG. 21 ANGULAR TWIST OF SHAFT BETWEEN GYRO DISKS DURING DECELERATION TEST

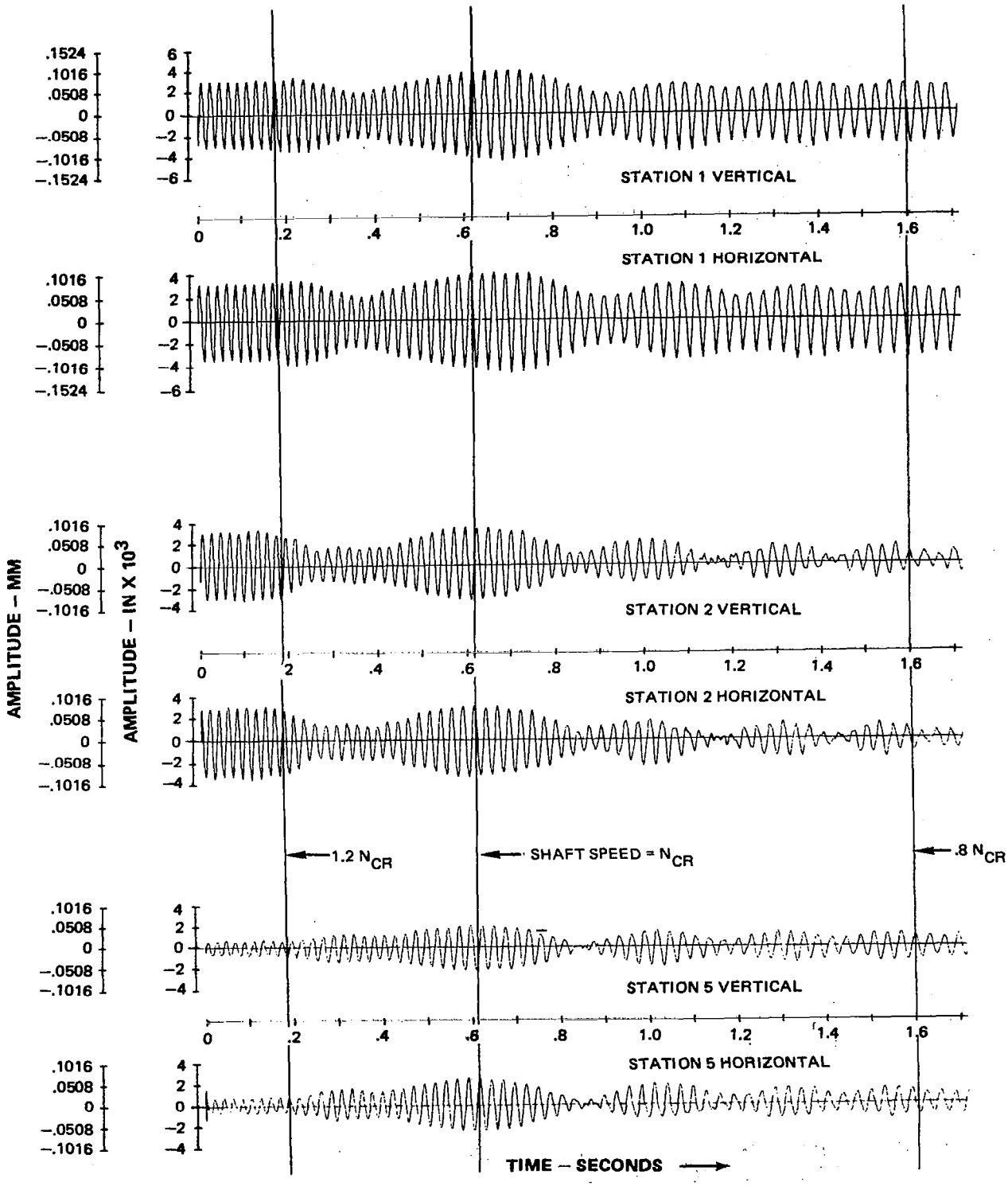

FIG. 22 DISPLACEMENT TIME TRACES FROM DATA STATIONS 1, 2 AND 5 DURING BALANCED DECELERATION TEST

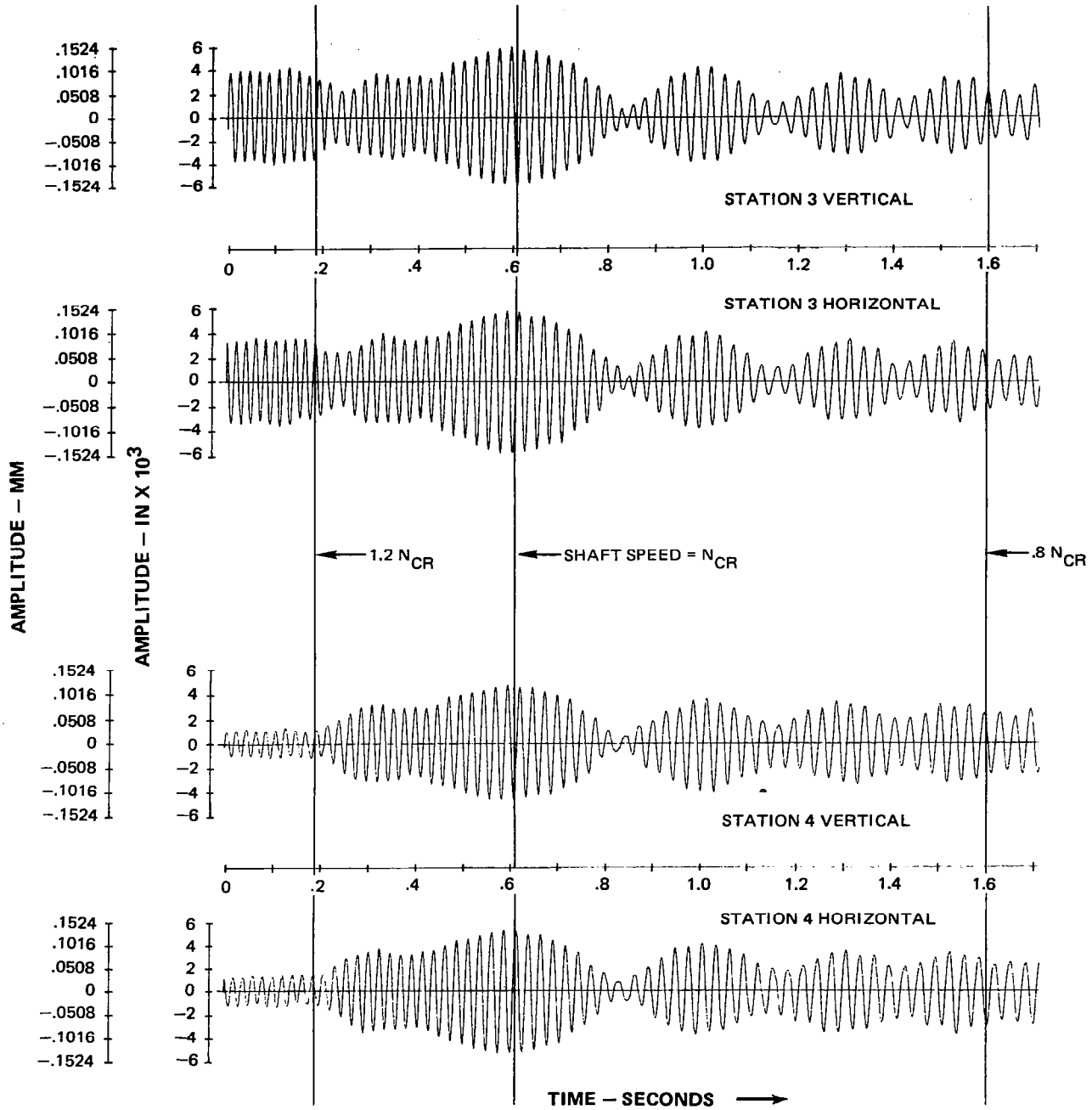

FIG. 23 **DISPLACEMENT TIME TRACES FROM DATA STATIONS 3 AND 4 DURING BALANCED DECELERATION TEST**

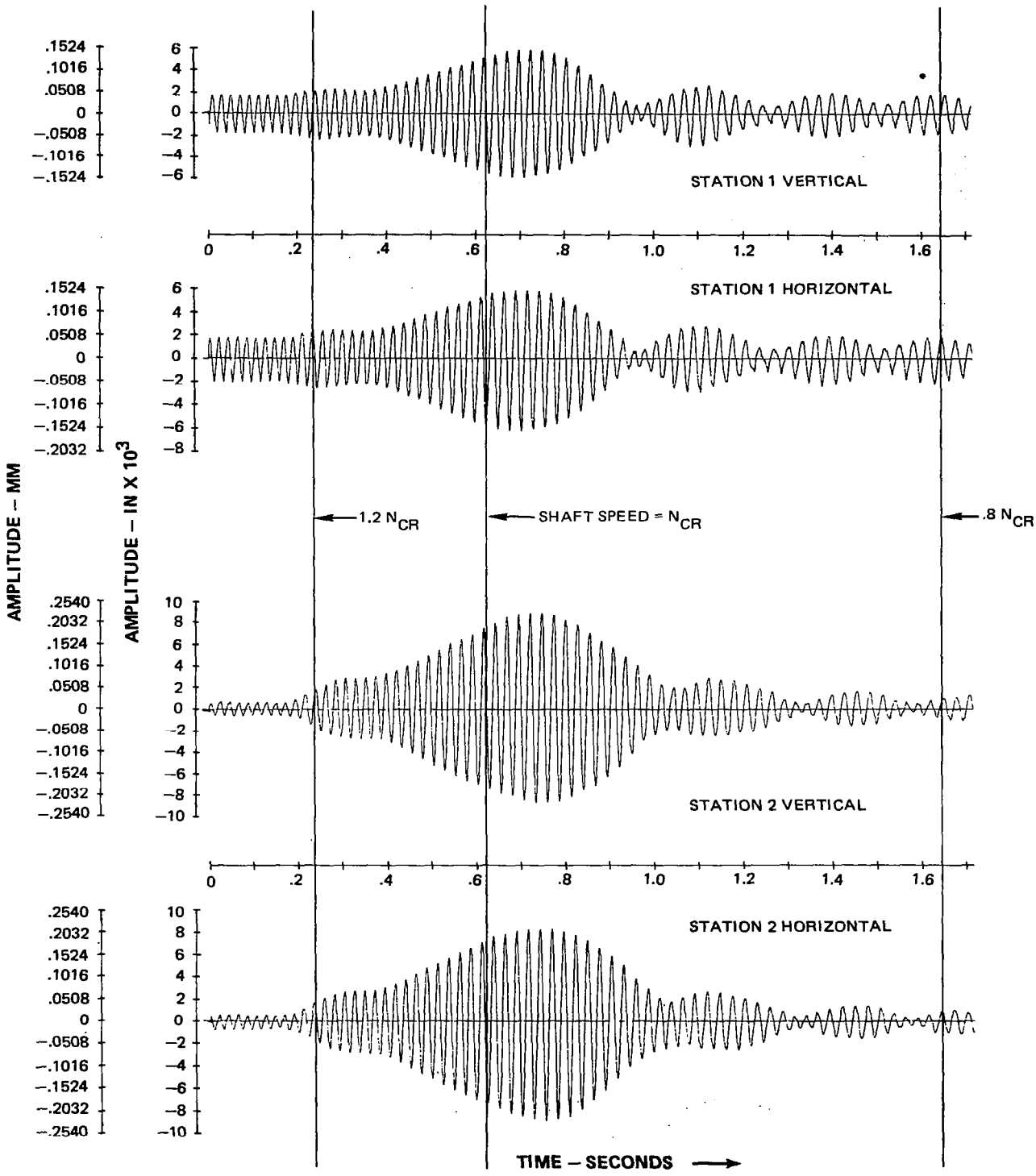

FIG. 24 DISPLACEMENT TIME TRACES FROM DATA STATIONS 1 AND 2 DURING UNBALANCED DECELERATION TEST

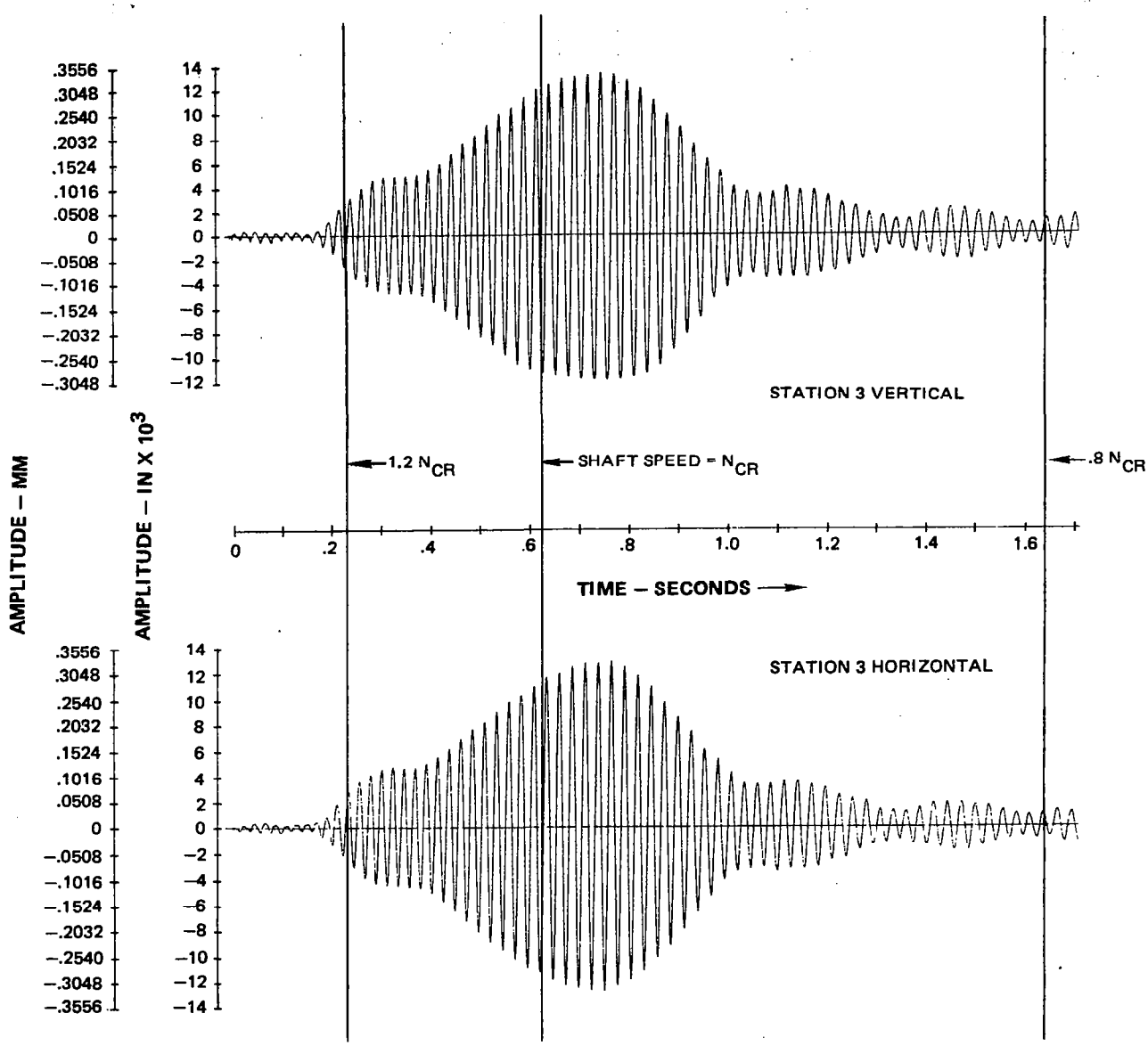

FIG. 25 DISPLACEMENT TIME TRACES FROM DATA STATION 3 DURING UNBALANCED DECELERATION TEST

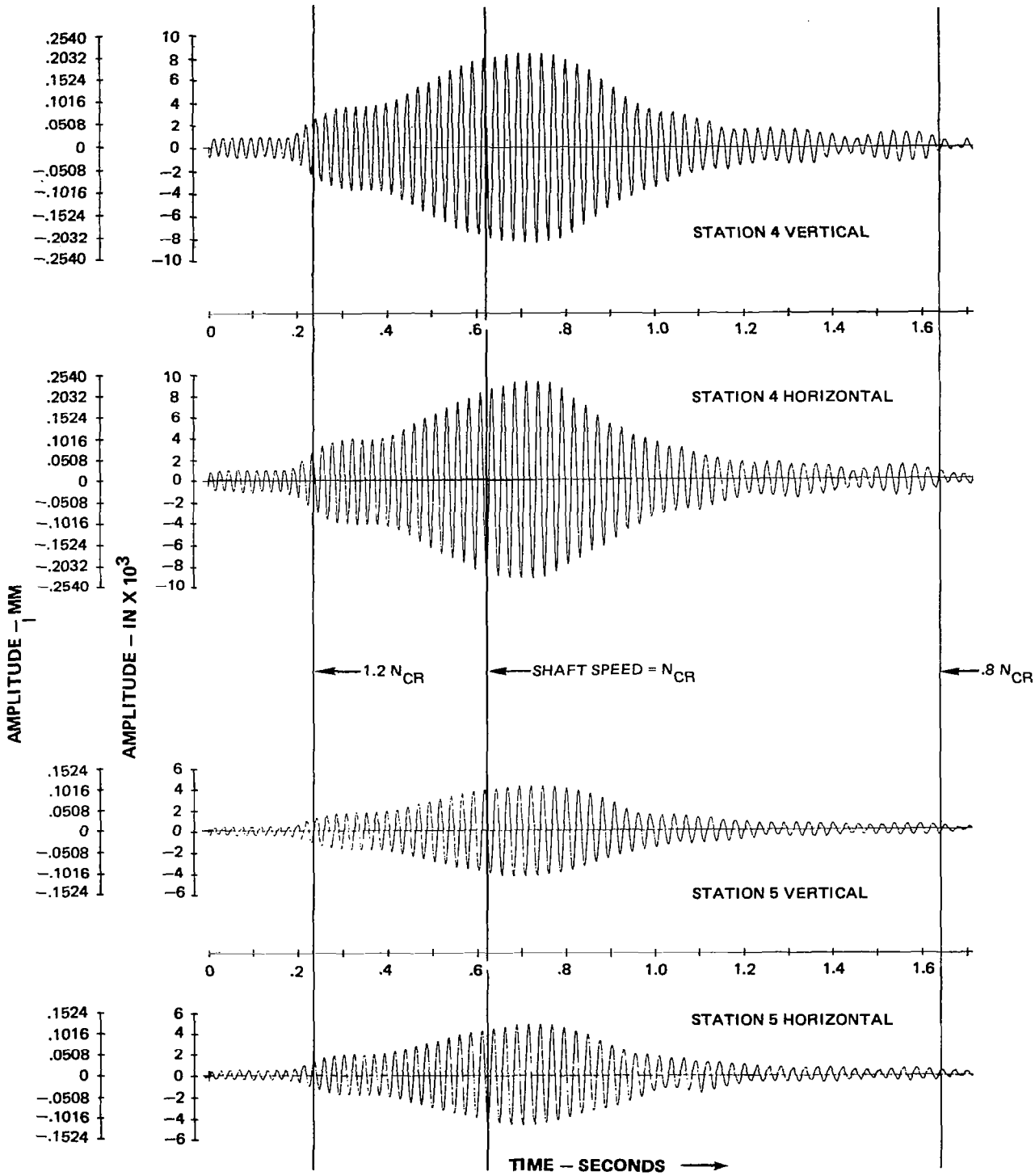

FIG. 26 DISPLACEMENT TIME TRACES FROM DATA STATIONS 4 AND 5 DURING UNBALANCED DECELERATION TEST

STATION 1 VERTICAL

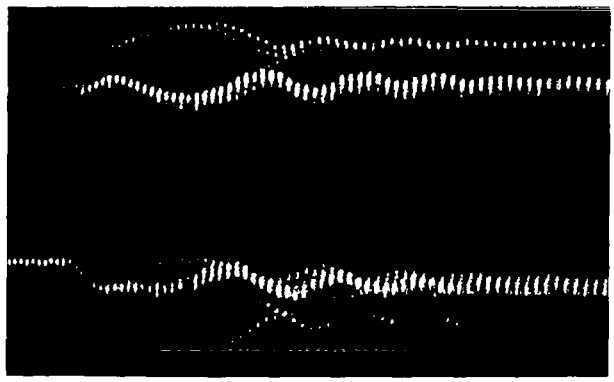

STATION 4 VERTICAL

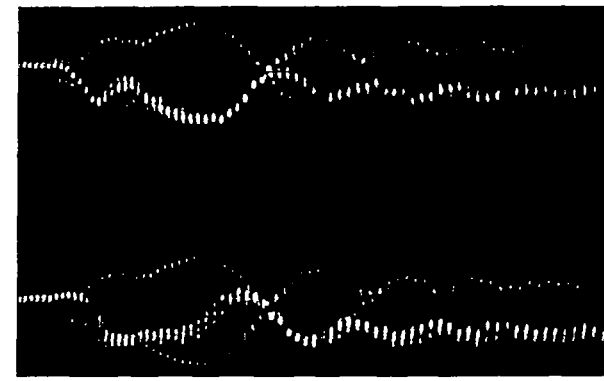

STATION 1 HORIZONTAL

STATION 4 HORIZONTAL

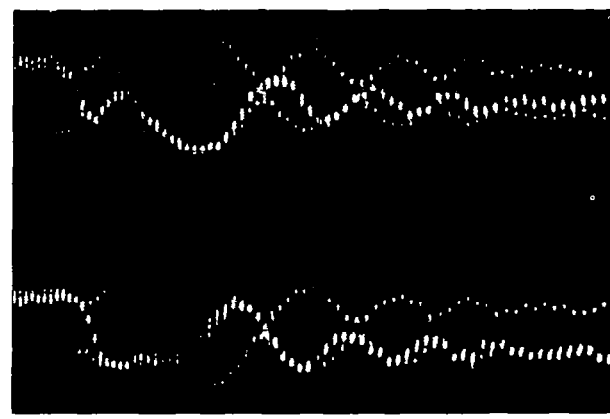

STATION 3 VERTICAL

STATION 3 HORIZONTAL

STATION 2 VERTICAL

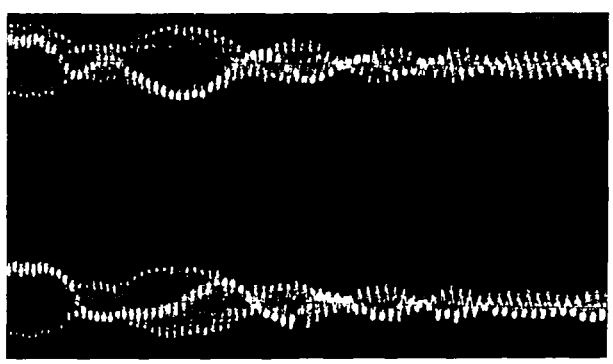

STATION 5 VERTICAL

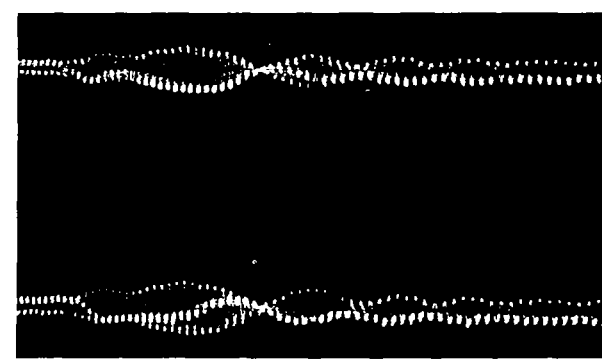

STATION 2 HORIZONTAL

STATION 5 HORIZONTAL

FIG. 27 DISPLACEMENT TIME TRACES WITH KEYPHASOR MARKS, DATA STATIONS 1, 2, 3, 4, AND 5 DURING BALANCED DECELERATION TEST

STATION 1 VERTICAL

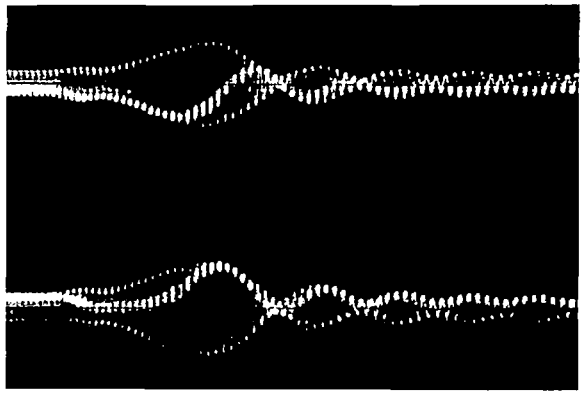

STATION 1 HORIZONTAL

STATION 4 VERTICAL

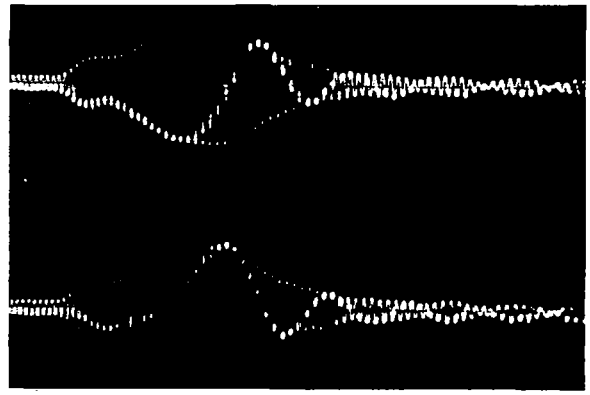

STATION 4 HORIZONTAL

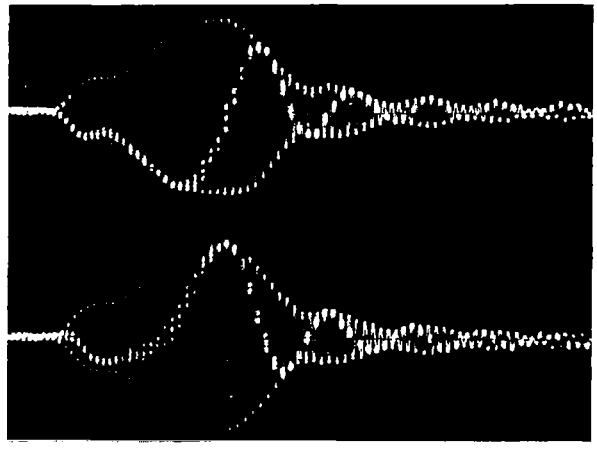

STATION 3 VERTICAL

STATION 3 HORIZONTAL

STATION 2 VERTICAL

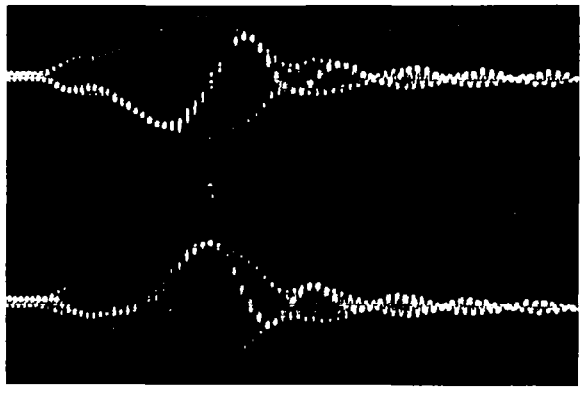

STATION 2 HORIZONTAL

STATION 5 VERTICAL

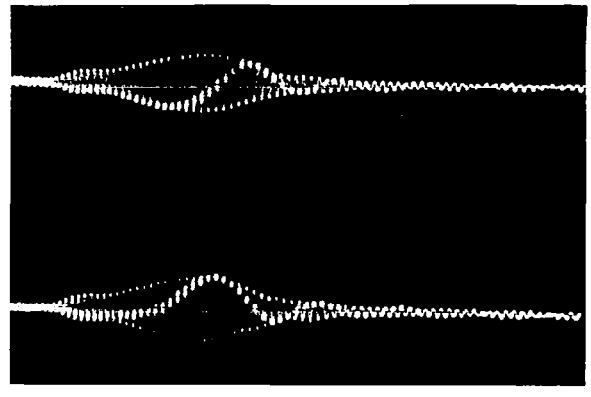

STATION 5 HORIZONTAL

FIG. 30 DISPLACEMENT TIME TRACES WITH KEYPHASOR MARKS, DATA STATIONS 1, 2, 3, 4 AND 5 DURING UNBALANCED DECELERATION TEST